Tada, M., Smith, J.C., 2000. Xwnt11 is a target of Xenopus Brachyury: regulation of gastrulation movements via Dishevelled, but not through the canonical Wnt pathway. Development 127, 2227–2238.

Taylor, M.E., Drickamer, K., 2007. Paradigms for glycan-binding receptors in cell adhesion. Curr. Opin. Cell. Biol. 19, 572–577.

Topczewski, J., Sepich, D.S., Myers, D.C., Walker, C., Amores, A., Lele, Z., Hammerschmidt, M., Postlethwait, J., Solnica-Krezel, L., 2001. The zebrafish glypican knypek controls cell polarity during gastrulation movements of convergent extension. Dev. Cell 1, 251–264.

Trinkaus, J.P., 1998. Gradient in convergent cell movement during Fundulus gastrulation. J. Exp. Zool. 281, 328–335.

Trinkaus, J.P., Trinkaus, M., Fink, R.D., 1992. On the convergent cell movements of gastrulation in Fundulus. J. Exp. Zool. 261, 40–61.

Umbhauer, M., Penzo-Mendez, A., Clavilier, L., Boucaut, J., Riou, J., 2000. Signaling specificities of fibroblast growth factor receptors in early Xenopus embryo. J. Cell Sci. 113 (Pt 16), 2865–2875.

Veeman, M.T., Slusarski, D.C., Kaykas, A., Louie, S.H., Moon, R.T., 2003. Zebrafish prickle, a modulator of noncanonical Wnt/Fz signaling, regulates gastrulation movements. Curr. Biol. 13, 680–685.

Winter, C.G., Wang, B., Ballew, A., Royou, A., Karess, R., Axelrod, J.D., Luo, L., 2001. Drosophila Rho-associated kinase (Drok) links Frizzled-mediated planar cell polarity signaling to the actin cytoskeleton. Cell 105, 81–91.

Yamamoto, A., Amacher, S.L., Kim, S.H., Geissert, D., Kimmel, C.B., De Robertis, E.M., 1998. Zebrafish paraxial protocadherin is a downstream target of spadetail involved in morphogenesis of gastrula mesoderm. Development 125, 3389–3397.

Yamamoto, T., 1954. Physiological studies on fertilization and activation of fish eggs. V. The role of calcium ions in activation of Oryzias eggs. Exp. Cell Res. 6, 56–68.

Zhao, H., Liang, Y., Xu, Z., Wang, L., Zhou, F., Li, Z., Jin, J., Yang, Y., Fang, Z., Hu, Y., Zhang, L., Su, J., Zha, X., 2007. N-Glycosylation affects the adhesive function of E-Cadherin through modifying the composition of adherens junctions (AJs) in human breast carcinoma cell line MDA-MB-435. J. Cell Biochem.

THE JOURNAL OF BIOLOGICAL CHEMISTRY VOL. 284, NO. 18, pp. 12550–12561, May 1, 2009


# Learning/Memory Impairment and Reduced Expression of the HNK-1 Carbohydrate in β4-Galactosyltransferase-II-deficient Mice*[S]

Received for publication, December 8, 2008, and in revised form, March 5, 2009 Published, JBC Papers in Press, March 5, 2009, DOI 10.1074/jbc.M809188200

**Toru Yoshihara**[‡§¶1], **Kazushi Sugihara**[‡1], **Yasuhiko Kizuka**[‖], **Shogo Oka**[**], **and Masahide Asano**[‡§2]

*From the [‡]Division of Transgenic Animal Science, Advanced Science Research Center, Kanazawa University, Kanazawa 920-8640, the [‖]Department of Biological Chemistry, Graduate School of Pharmaceutical Sciences, Kyoto University, Kyoto 606-8501, the [**]Department of Biological Chemistry, Human Health Science, Graduate School of Medicine, Kyoto University, Kyoto 606-8507, the [§]Kanazawa University 21st Century COE Program on Innovative Brain Science on Development, Learning, and Memory, Kanazawa 920-8640, and the [¶]Kanazawa University Research Center for Child Mental Development, Kanazawa 920-8640, Japan*

**The glycosylation of glycoproteins and glycolipids is important for central nervous system development and function. Although the roles of several carbohydrate epitopes in the central nervous system, including polysialic acid, the human natural killer-1 (HNK-1) carbohydrate, α2,3-sialic acid, and oligomannosides, have been investigated, those of the glycan backbone structures, such as Galβ1–4GlcNAc and Galβ1–3GlcNAc, are not fully examined. Here we report the generation of mice deficient in β4-galactosyltransferase-II (β4GalT-II). This galactosyltransferase transfers Gal from UDP-Gal to a nonreducing terminal GlcNAc to synthesize the Galβ1–4GlcNAc structure, and it is strongly expressed in the central nervous system. In behavioral tests, the β4GalT-II$^{-/-}$ mice showed normal spontaneous activity in a novel environment, but impaired spatial learning/memory and motor coordination/learning. Immunohistochemistry showed that the amount of HNK-1 carbohydrate was markedly decreased in the brain of β4GalT-II$^{-/-}$ mice, whereas the expression of polysialic acid was not affected. Furthermore, mice deficient in glucuronyltransferase (GlcAT-P), which is responsible for the biosynthesis of the HNK-1 carbohydrate, also showed impaired spatial learning/memory as described in our previous report, although their motor coordination/learning was normal as shown in this study. Histological examination showed abnormal alignment and reduced number of Purkinje cells in the cerebellum of β4GalT-II$^{-/-}$ mice. These results suggest that the Galβ1–4GlcNAc structure in the HNK-1 carbohydrate is mainly synthesized by β4GalT-II and that the glycans synthesized by β4GalT-II have essential roles in higher brain functions, including some that are HNK-1-dependent and some that are not.**

The glycosylation of glycoproteins, proteoglycans, and glycolipids is important for their biological activities, stability, transport, and clearance from circulation, and cell-surface glycans participate in cell-cell and cell-extracellular matrix interactions. In the central nervous system, several specific carbohydrate epitopes, including polysialic acid (PSA),[3] the human natural killer-1 (HNK-1) carbohydrate, α2,3-sialic acid, and oligomannosides play indispensable roles in neuronal generation, cell migration, axonal outgrowth, and synaptic plasticity (1). Functional analyses of the glycan backbone structures, like lactosamine core (Galβ1–4GlcNAc), neolactosamine core (Galβ1–3GlcNAc), and polylactosamine (Galβ1–4GlcNAcβ1–3) have been carried out using gene-deficient mice in β4-galactosyltransferase-I (β4GalT-I) (2, 3), β4GalT-V (4), β3-*N*-acetylglucosaminyltransferase-II (β3GnT-II) (5), β3GnT-III (Core1-β3GnT) (6), β3GnT-V (7), and Core2GnT (8). However, the roles of these glycan backbone structures in the nervous system have not been examined except the olfactory sensory system (9).

β4GalTs synthesize the Galβ1–4GlcNAc structure via the β4-galactosylation of glycoproteins and glycolipids; the β4GalTs transfer galactose (Gal) from UDP-Gal to a nonreducing terminal *N*-acetylglucosamine (GlcNAc) of *N*- and *O*-glycans with a β-1,4-linkage. The β4GalT family has seven members (β4GalT-I to VII), of which at least five have similar Galβ1–4GlcNAc-synthesizing activities (10, 11). Each β4GalT has a tissue-specific expression pattern and substrate specificity with overlapping, suggesting each β4GalT has its own biological role as well as redundant functions. β4GalT-I and β4GalT-II share the highest identity (52% at the amino acid level) among the β4GalTs (12), suggesting these two galactosyltransferases can compensate for each other. β4GalT-I is strongly and ubiquitously expressed in various non-neural tissues, whereas β4GalT-II is strongly expressed in neural tissues (13, 14). Indeed, the β4GalT activity in the brain of β4GalT-I-deficient (β4GalT-I$^{-/-}$) mice remains as high as 65% of that of wild-type mice, and the expression levels of PSA and the HNK-1 carbohydrate in the brain of these mice are normal (15). These results

* This work was supported in part by Grant-in-aid 19300144 and the 21st Century COE Program K-1 from the Ministry of Education, Culture, Sports, Science and Technology of Japan.

[S] The on-line version of this article (available at http://www.jbc.org) contains supplemental Fig. 1.

[1] Both authors contributed equally to this work.

[2] To whom correspondence should be addressed: 13-1 Takara-machi, Kanazawa 920-8640, Japan. Tel.: 81-76-265-2460; Fax: 81-76-234-4240; E-mail: asano@kiea.m.kanazawa-u.ac.jp.

[3] The abbreviations used are: PSA, polysialic acid; HNK-1, human natural killer-1; β4GalT, β4-galactosyltransferase; GlcAT-P, glucuronyltransferase; mAb, monoclonal antibody; DG, dentate gyrus; BrdUrd, 5-bromo-2′-deoxyuridine; HRP, horseradish peroxidase; PBS, phosphate-buffered saline; NCAM, neural cell adhesion molecule.

suggest β4GalTs other than β4GalT-I, like β4GalT-II, are important in the nervous system.

Among the β4GalT family members, only β4GalT-I$^{-/-}$ mice have been examined extensively; this was done by us and another group. We reported that glycans synthesized by β4GalT-I play various roles in epithelial cell growth and differentiation, inflammatory responses, skin wound healing, and IgA nephropathy development (2, 16–18). Another group reported that glycans synthesized by β4GalT-I are involved in anterior pituitary hormone function and in fertilization (3, 19). However, no other nervous system deficits have been reported in these mice, and the role of the β4-galactosylation of glycoproteins and glycolipids in the nervous system has not been fully examined.

In this study, we generated β4GalT-II$^{-/-}$ mice and examined them for behavioral abnormalities and biochemical and histological changes in the central nervous system. β4GalT-II$^{-/-}$ mice were impaired in spatial learning/memory and motor coordination/learning. The amount of HNK-1 carbohydrate was markedly decreased in the β4GalT-II$^{-/-}$ brain, but PSA expression was not affected. These results suggest that the Galβ1–4GlcNAc structure in the HNK-1 carbohydrate is mainly synthesized by β4GalT-II and that glycans synthesized by β4GalT-II have essential roles in higher brain functions, including ones that are HNK-1 carbohydrate-dependent and ones that are independent of HNK-1.

## EXPERIMENTAL PROCEDURES

*Generation of β4GalT-II$^{-/-}$ Mice*—The strategy for the β4GalT-II gene targeting was to replace exons 1 and 2 and part of exon 3 with the neomycin resistance gene (20). Because exon 2 contains the translation initiation codon, ATG, as well as the Golgi retention signal, the deletion of exon 2 was expected to result in null function. A targeting vector with an upstream DT-A cassette (21) was used to transfect E14-1 embryonic stem cells (22) by electroporation, and the transformed cells were selected with G418 (2). Disruption of the β4GalT-II gene was verified by Southern blot hybridization using external 5′ and 3′ probes. Chimeric mice were generated by the aggregation method (23) and mated to C57BL/6 mice to confirm germ line transmission. The absence of β4GalT-II gene expression in the homozygous mutant mice was confirmed by Northern blot hybridization using a specific probe and by reverse transcription-PCR with a primer set that detected the deleted region. The mice used for the experiments were obtained by crossbreeding male homozygous and female heterozygous mutant mice. In most cases, mice backcrossed to the C57BL/6J strain for eight generations were used in the behavioral analyses, and other experiments were carried out using mice of a mixed 129/Ola × C57BL/6J background. The exceptional cases are described under "Results."

*Preparation of Brain Homogenate and Membrane Fraction*—Whole brains from postnatal day 0 (P0), 2-week-old, and 11-week-old mice were homogenized with a Polytron homogenizer in 9 volumes of 20 mM Tris-HCl (pH 7.4) containing 150 mM NaCl, 1 mM EDTA, and protease inhibitors (Nacalai Tesque, Kyoto, Japan). The homogenate was spun at 1,000 × *g* for 10 min at 4 °C to remove the nuclei and then spun again at 105,000 × *g* for 1 h at 4 °C, and the resulting pellet was used as the membrane fraction. After being resuspended in PBS, the protein concentration in the homogenate and membrane fraction was measured using the DC-Protein Assay Reagent (Bio-Rad), according to the manufacturer's protocol.

*SDS-PAGE, Western Blot, and Lectin Blot*—Western blotting and lectin blotting were carried out as described previously (24). Proteins were separated by 5–20% gradient SDS-PAGE using the Laemmli buffer system and then transferred to nitrocellulose membranes. For Western blots, after being blocked with 5% skim milk (or, for the detection of PSA, 2% bovine serum albumin) in PBS containing 0.05% Tween 20, the membranes were incubated with primary antibodies followed by incubation with HRP-conjugated secondary antibodies. For lectin blots, after being blocked with 0.1% Tween 20 in TBS (T-TBS), the membranes were incubated with HRP- or biotin-conjugated lectins in T-TBS. To detect biotinylated lectins, we used the Vectastain-ABC kit (Vector Laboratories), according to the manufacturer's protocol. Protein bands were detected with SuperSignal West Pico (Pierce) using a Luminoimage Analyzer LAS-3000 (Fuji, Tokyo, Japan). In these analyses, an anti-HNK-1 monoclonal antibody (mAb) was purchased from American Type Culture Collection, Manassas, VA; the anti-polysialic acid mAb (clone 12E3) was a generous gift from Dr. T. Seki (Juntendo University). The rat anti-mouse neural cell adhesion molecule (NCAM) mAb (clone H28) was kindly provided by Dr. K. Ono (National Institute for Physiological Sciences). The fluorescein isothiocyanate-conjugated anti-mouse IgM was purchased from Cappel Laboratories, and the HRP-conjugated anti-mouse IgM, anti-rabbit IgG, and anti-rat IgG were obtained from Zymed Laboratories Inc.. Biotinylated lectins (*Maackia amurensis* agglutinin and *Sambucus sieboldiana* agglutinin) and HRP-conjugated lectins (concanavalin A and RCA120) were purchased from Seikagaku Corp., Tokyo, Japan. Concanavalin A, RCA120 (*Ricinus communis* agglutinin), *M. amurensis* agglutinin, and *S. sieboldiana* agglutinin recognized mannose, Galβ1–4GlcNAc, Siaα2–3Gal, and Siaα2–6Gal, respectively.

*Histological Procedures*—Two-week- and 11-week-old and 2-month- and 6-month-old mice were deeply anesthetized with diethyl ether and perfused with PBS containing 0.1% heparin and then with 4% paraformaldehyde in PBS. The brain was post-fixed overnight and then sunk in 30% sucrose solution or embedded in paraffin. Cryo- or paraffin sections were cut in the sagittal or coronal plane. For a broad morphologic investigation, Kluver-Barrera's stain was used with 0.1% Luxol Fast Blue and 0.1% Cresyl Violet solutions.

*Immunohistochemistry*—Immunohistochemistry was used to investigate the morphologic features of neural cells, the number of each cell type, and their glycosylation status. The primary antibodies were as follows: anti-HNK-1 mAb (TIB-20; ATCC, Manassas, VA); anti-PSA mAb (12E3); anti-NeuN mAb (MAB377; Chemicon, CA); anti-Nestin mAb (MAB353; Chemicon, CA); and anti-calbindin D-28K mAb (CB-955; C9848, Sigma). Sections were incubated with primary antibodies overnight at 4 °C, rinsed twice in PBS, and then incubated with Alexa Fluor-488- or fluorescein isothiocyanate-conjugated secondary antibody for 2 h at room temperature. Immu-

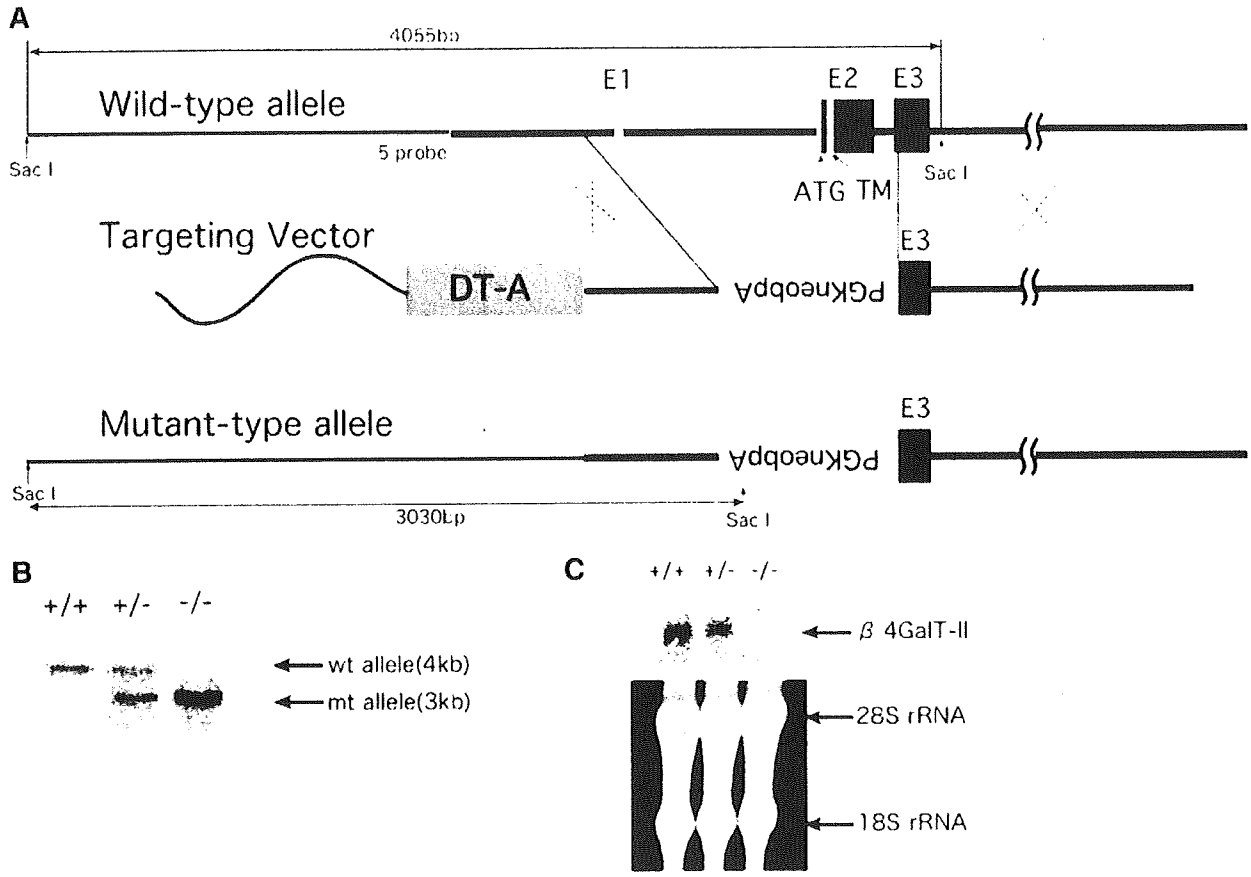


FIGURE 1. **Generation of β4GalT-II-deficient mice by gene targeting.** *A*, schematic figure of the targeting strategy. Exon 1 (*E1*), exon 2 (*E2*), and part of exon 3 (*E3*) of the *β4GalT-II* gene were replaced by the neomycin resistance gene cassette (PGKneobpA). *ATG*, translation initiation codon; *TM*, transmembrane domain; *DT-A*, diphtheria toxin A fragment cassette. *B*, Southern blot hybridization analysis. Genomic DNA from the liver of each mouse was digested with SacI and hybridized with the 5′ probe shown in *A*. *wt*, wild type; *mt*, mutant. *C*, Northern blot hybridization analysis. β4GalT-II mRNA was not detected in the brain of the β4GalT-II$^{-/-}$ mouse.

nofluorescence was evaluated by confocal microscopy (LSM 5 Pascal, Zeiss, Oberkochen, Germany; Fluoview laser confocal microscope system, Olympus Corp., Tokyo, Japan). For the calbindin D-28K immunohistochemical staining, the number of calbindin-positive cells in the 4th and 5th cerebellar lobules was counted manually. Disturbed alignment of cerebellar Purkinje cells was evaluated by counting the number of disturbed lobules using the sections in which apparent eight lobules were observed. For this quantitative analysis, five sagittal sections (0.12–0.84 mm lateral to the midline) (25) per animal were investigated, and the total number of 40 lobules in an animal (five sections by eight lobules) was examined. For the assessment of BrdUrd incorporation, 100 mg/kg BrdUrd solution was injected once a day intraperitoneally for 5 days, and the animals were perfused intracardially 24 h after the last injection. BrdUrd immunostaining was carried out using a BrdUrd labeling and detection kit II (Roche Diagnostics), and the sections were counterstained with nuclear fast red.

*Behavioral Tests, General Procedures*—Three-month-old male β4GalT-II$^{-/-}$ mice ($n$ = 15), β4GalT-II$^{+/+}$ littermates ($n$ = 13), GlcAT-P$^{-/-}$ mice ($n$ = 11), and GlcAT-P$^{+/+}$ mice ($n$ = 9), kept under specific pathogen-free conditions at the Institute for Experimental Animals (Advanced Science Research Center, Kanazawa University), were used for behavioral analyses. The subjects were housed individually with *ad libitum* access to food and water 1 week before the behavioral testing. All tests were conducted during the light period of the light/dark cycle (08:45–20:45 h). To evaluate the behavioral responses in every test situation, the products of O'Hara & Co., Ltd. (Tokyo, Japan) were used. In addition, for the quantitative analysis in the open field and Morris water maze test, we used ImageJ LD4 (O'Hara & Co., Ltd.), a modified software based on the public domain ImageJ program (developed at the National Institutes of Health and available on line at www.nih.gov). Each animal was subjected to a battery of the following five behavioral paradigms with an ~1-week rest period between each test. The animal experiments were conducted according to Fundamental Guidelines for Proper Conduct of Animal Experiment and Related Activities in Academic Research Institutions under the jurisdiction of the Ministry of Education, Culture, Sports, Science and Technology of Japan, and to the safety guidelines for gene manipulation experiments at Kanazawa University. All efforts were made to minimize both the number and the suffering of the animals used.

*Open Field Test*—The general activity of animals in a novel environment was measured in an open field situation. The open

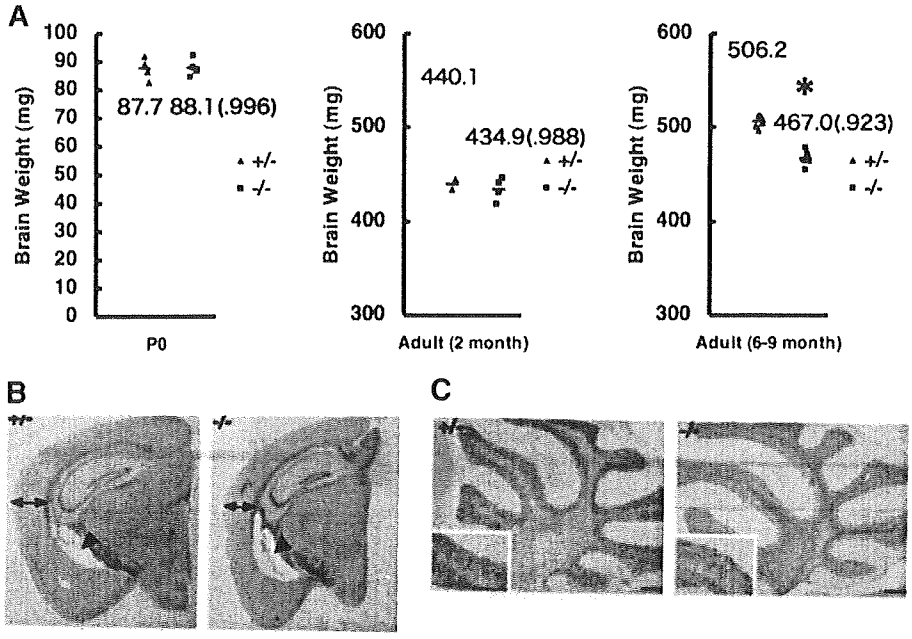


FIGURE 2. **Morphology of the brain.** *A*, brain weight was significantly reduced in β4GalT-II $^{-/-}$ mice at 6–9 months old (*, $p < 0.05$, *t* test). The whole brain weight of each P0 (±, $n = 4$; −/−, $n = 4$), 2-month-old (±, $n = 2$; −/−, $n = 4$), and 6–9-month-old (±, $n = 5$; −/−, $n = 5$) mouse was measured. *B*, Kluver-Barrera's staining of coronal sections of the cerebral cortex. Reduced cortex (*arrow*) and enlargement of the lateral ventricle (*arrowhead*) were seen in the β4GalT-II $^{-/-}$ mice at 8 months old. In the cerebellum (*C*), no morphologic differences were observed among the genotypes.

field chamber (60 × 60 × 40 cm) was made of gray vinyl chloride, and the illumination of the center of the floor was kept at 50 lux by white LEDs set just above the chamber. The mice were allowed free exploration of the apparatus for 10 min per day on 3 successive days. The moving distance, speed, staying area, and number of rearing were analyzed.

*Morris Water Maze Task*—The Morris water maze task (26) was used to evaluate spatial learning. The apparatus consisted of a pool (100 cm in diameter) filled with opaque water (23 ± 2 °C) and containing a submerged hidden goal platform (10 cm in diameter) 1 cm below the surface of the water. Mice were given six training trials (inter-trial interval, 10–15 min) per day for 8 consecutive days. The trials were initiated from each of four possible start locations in a randomized manner, and the mice were required to reach the platform within 60 s. Following 2 days of extinction trials, a "landmark task," with a visible cue on the platform was carried out to determine visual impairment. The latency to reach the platform and the length of the swimming pass were analyzed as learning performance.

*Passive Avoidance Response*—The passive avoidance apparatus consisted of a vinyl chloride chamber (30 × 10 × 9 cm) with a steel-grid floor that was divided into dark and light compartments. In the test trial, mice were placed in the light room and received scrambled electrical foot shocks (0.22 mA) for 5 s through the grid floor of the dark room when they entered it. To test memory retention, each animal was again placed into the light room 24 h after the training. The step-through latency was measured without electric foot shocks as an indicator of the memory of shock experience. An upper cutoff of 300 s was set.

*Rota-rod Test*—To investigate the motor coordination/motor learning abilities, the accelerating rota-rod paradigm (27) was used. Animals were tested in three trials per day for 3 consecutive days with a 300-s accelerating program (from 5 to 40 rpm). The latency to fall from the rod was recorded. On day 4, the number of hind limb steps at 7 rpm was measured to examine whether there was a motility defect.

*Balance Beam Test*—Motor coordination and balance were evaluated by a balance beam apparatus (28). The beam consisted of a 100-cm-long horizontal steel bar (28 or 11 mm in diameter) placed 50 cm above the floor. Following the habituation trials, the mice were placed at the starting point of the bar. The number of hind limb slips off the beam before reaching an enclosed goal box was counted. Every mouse was tested using both bar diameters.

*Statistical Analysis*—In the behavioral experiments statistical significance was determined by two-way analysis of variance followed by a post hoc protected least significant difference test or unpaired *t* test. Performance in the open field test and Morris water maze task was analyzed by two-way analysis of variance in which the trial/day effect was a within-subject factor and genotype was a between-subject factor. In the other behavioral tests, the effect of genotype was verified by the *t* test.

## RESULTS

*Generation of β4GalT-II $^{-/-}$ Mice*—The targeting strategy for the deletion of the *β4GalT-II* gene is shown in Fig. 1*A*. The targeting vector was introduced into E14-1 embryonic stem cells by electroporation, and G-418-resistant colonies were picked up. Three embryonic stem clones were selected by Southern blot screening of 600 colonies and were verified to have the desired homologous recombination by Southern blot analysis (data not shown). β4GalT-II $^{-/-}$ mice were generated from two independent embryonic stem clones, and behavioral experiments were conducted using mice that had been backcrossed to C57BL/6 mice for eight generations. The targeted deletion of exons 1 and 2 of the *β4GalT-II* gene and the loss of β4GalT-II mRNA in the brain were confirmed by Southern (Fig. 1*B*) and Northern (Fig. 1*C*) blot analyses, respectively. In the heterozygous cross-breeding, β4GalT-II $^{-/-}$ mice were born at the expected Mendelian frequency, were fertile (data not shown), and exhibited no obvious behavioral phenotypes in an ordinary home-cage environment.

*Histological Features of the Brain*—The brain weight of β4GalT-II $^{-/-}$ mice on a C57BL/6 genetic background was nearly identical to that of the β4GalT-II $^{+/+}$ mice at least until 2 months of age. However, the brain weight was significantly reduced in the β4GalT-II $^{-/-}$ mice at 6–9 months of age (Fig.

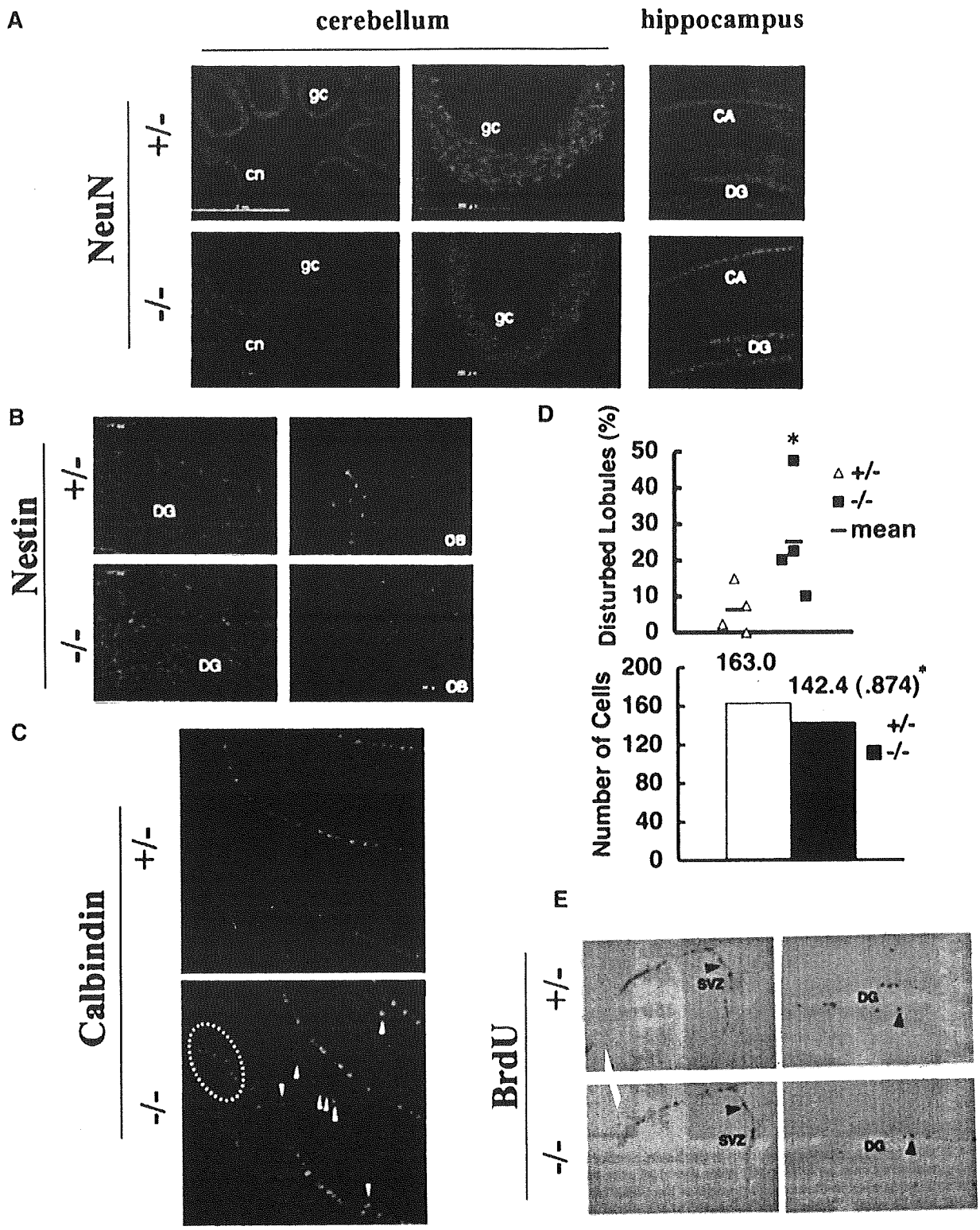


FIGURE 3. **Immunohistochemical analysis of the brain.** *A*, NeuN-positive neurons located in the cerebellar granular cell layer (*gc*), cerebellar nuclei (*cn*), and CA region/dentate gyrus (*DG*) of the hippocampus. *B*, Nestin-positive cells in the DG (*left*) and rostral migratory stream near the olfactory bulb (*OB*) (*right*) were the same in both genotypes. *C*, calbindin-positive Purkinje cells in the cerebellum. The section from a β4GalT-II$^{-/-}$ mouse shows ectopic Purkinje cells (*arrowheads*) and their disturbed alignment (*circled area*). *D*, *upper*, ratio of disturbed cerebellar lobules (total 40 lobules per a mouse) was counted (+/−, $n$ = 4; −/−, $n$ = 4). The β4GalT-II$^{-/-}$ mice had significantly more disturbed cerebellar lobules (*, $p < 0.05$). *D*, *lower*, number of Purkinje cells was significantly reduced in the mutant mice(+/ , $n$ = 4; −/−, $n$ = 4, *, $p < 0.05$). *E*, BrdUrd-labeled cells (*arrowhead*) in the subventricular zone (*SVZ*) and DG.

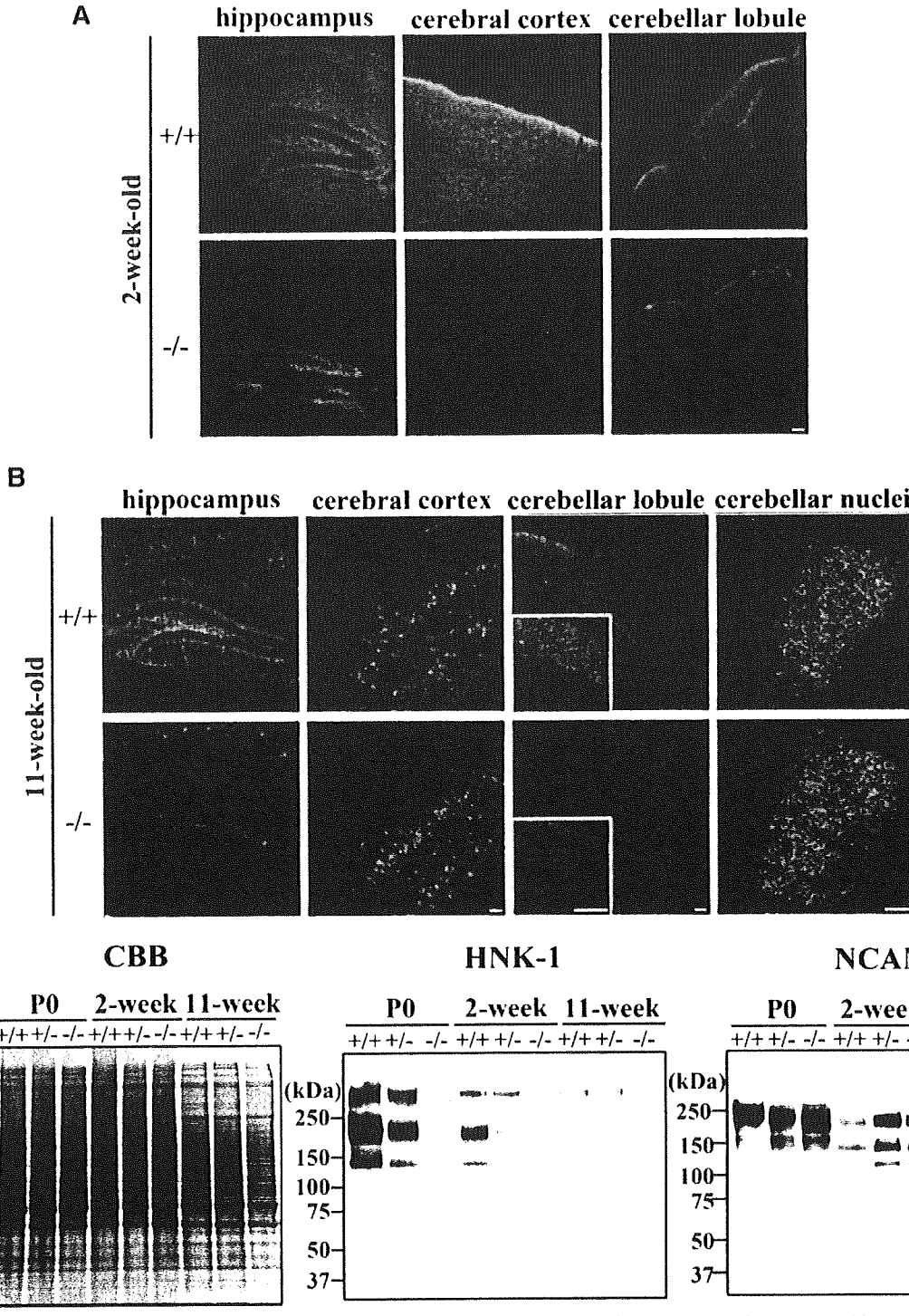


FIGURE 4. **HNK-1 carbohydrate expression in the brain.** Sections of the brain from β4GalT-II$^{+/+}$ and β4GalT-II$^{-/-}$ of 2-week-old (*A*) and 11-week-old mice (*B*) were immunostained with an anti-HNK-1 mAb (*bar*, 100 μm). HNK-1-positive signals were markedly decreased in the hippocampus, cerebral cortex, and cerebellar lobules but not in the cerebellar nuclei of the β4GalT-II$^{-/-}$ mice, at both developmental stages. *C*, brain membrane fractions from postnatal day 0, 2-week-old, and 11-week-old mice were subjected to SDS-PAGE and then to Coomassie Brilliant Blue (*CBB*) staining (*left panel*) or to Western blotting with the anti-HNK-1 mAb (*middle panel*) or with an anti-NCAM mAb (*right panel*). The HNK-1 immunoreactivity was decreased in the β4GalT-II$^{-/-}$ mice at all three ages. Twenty micrograms of protein were loaded in each lane.

2*A*). Kluver-Barrera's staining (Fig. 2, *B* and *C*) revealed that the thickness of the cerebral cortex was slightly reduced, and the lateral ventricle was enlarged in the 8-month-old β4GalT-II$^{-/-}$ mice, indicating that the cerebral cortex of these mice atrophied slightly with age. In the cerebellum, no prominent morphological differences were observed between the genotypes.

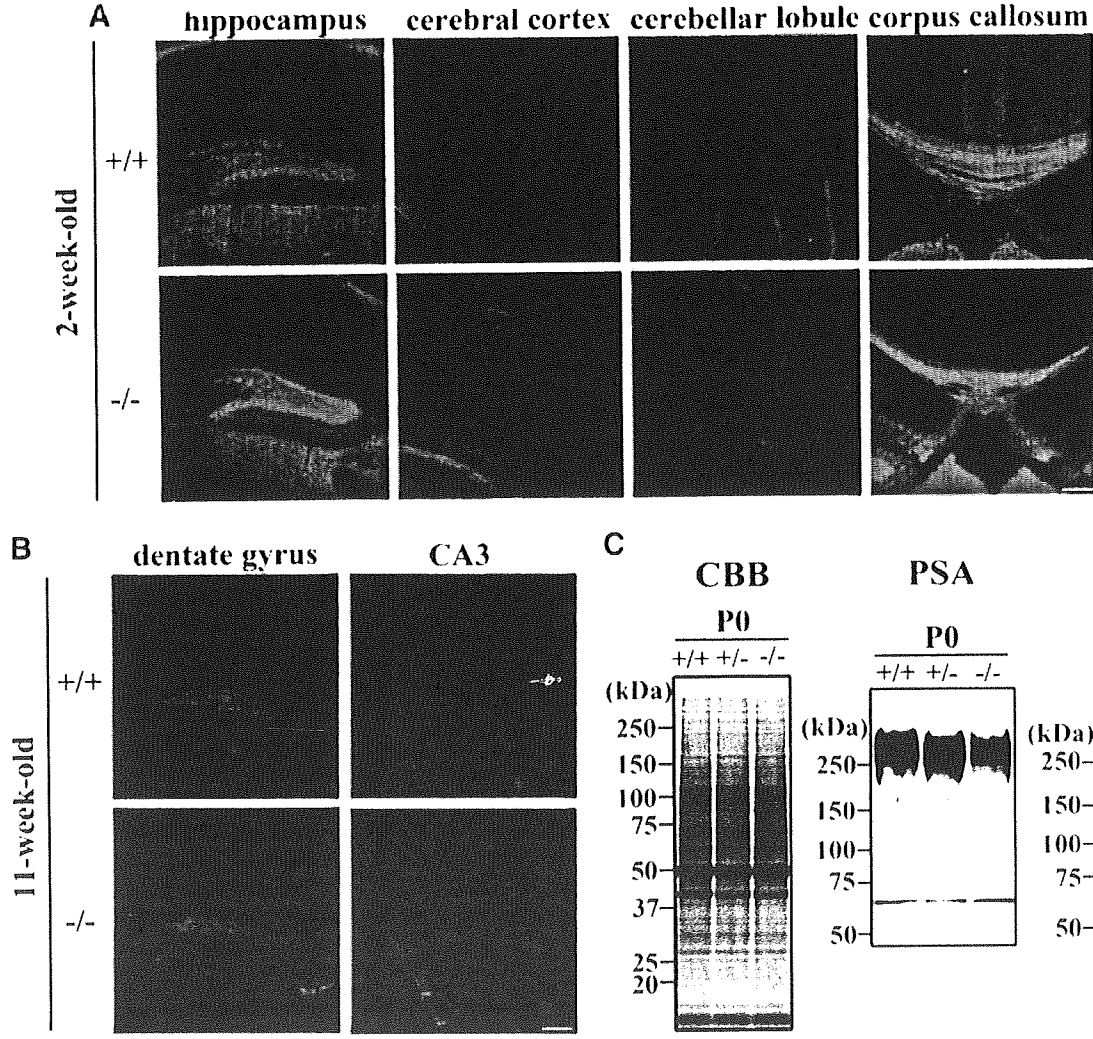


FIGURE 5. **PSA expression in the brain.** Sections of the brain from β4GalT-II$^{+/+}$ and β4GalT-II$^{-/-}$ of 2-week-old (*A*) and 11-week-old mice (*B*) were immunostained with an anti-PSA mAb (*bar*, 200 μm). C, brain membrane fractions from postnatal day 0 mice were subjected to SDS-PAGE and then to Coomassie Brilliant Blue (*CBB*) staining (*left panel*) or Western blotting with the anti-PSA mAb (*middle panel*) or with an anti-NCAM mAb (*right panel*). Thirty micrograms of protein were loaded in each lane.

Brain sections from adult mice were immunostained with several neuronal markers. NeuN-positive mature neurons were appropriately located in the cerebellar granular cell layer, cerebellar nuclei, and CA region/dentate gyrus (DG) of the hippocampus in both the β4GalT-II$^{+/-}$ and β4GalT-II$^{-/-}$ mice (Fig. 3*A*). Nestin-positive neural progenitor cells were present in the DG and rostral migratory stream near the olfactory bulb in both genotypes (Fig. 3*B*). In the cerebellum of the β4GalT-II$^{-/-}$ mice, however, several calbindin-positive Purkinje cells were ectopically located, and their alignment was partially disturbed (Fig. 3*C*). Quantitative analysis showed that the β4GalT-II$^{-/-}$ mice had significantly more disturbed cerebellar lobules than β4GalT-II$^{+/-}$ mice (Fig. 3*D*, *upper*). In addition, the number of Purkinje cells was significantly reduced in the 4th and 5th cerebellar lobules of the β4GalT-II$^{-/-}$ mice compared with β4GalT-II$^{+/-}$ mice (Fig. 3*D*, *lower*). In the subventricular zone and DG of the hippocampus of the β4GalT-II$^{-/-}$ mice, the pattern of BrdUrd-labeled cells was the same as in the β4GalT-II$^{+/-}$ mice (Fig. 3*E*).

*Reduced Expression of the HNK-1 Carbohydrate in the β4GalT-II$^{-/-}$ Mouse Brain*—Because the HNK-1 carbohydrate and PSA, which are well known functional carbohydrates in the nervous system, are expressed on the β4-galactose epitope, we investigated the expression of these carbohydrates in the β4GalT-II$^{-/-}$ mouse brain. Immunohistochemical staining with an anti-HNK-1 antibody revealed strong and widespread expression of the HNK-1 carbohydrate in the 2-week-old β4GalT-II$^{+/+}$ mouse brain, including the cerebral cortex and hippocampus, and comparatively less expression in the cerebellum (Fig. 4*A*). In contrast, the immunoreactivity of the HNK-1 carbohydrate in the 2-week-old β4GalT-II$^{-/-}$ mice was markedly reduced in the cerebral cortex and hippocampus. In the 11-week-old β4GalT-II$^{-/-}$ mouse brain (Fig. 4*B*), the HNK-1 reactivity was barely detectable only in the DG of the hippocampus, layers III–IV of the cerebral cortex, and the cerebellar lobule. In the cerebellar nuclei of the β4GalT-II$^{-/-}$ mice, no reduction of the HNK-1 carbohydrate was apparent, in contrast to the other brain regions.

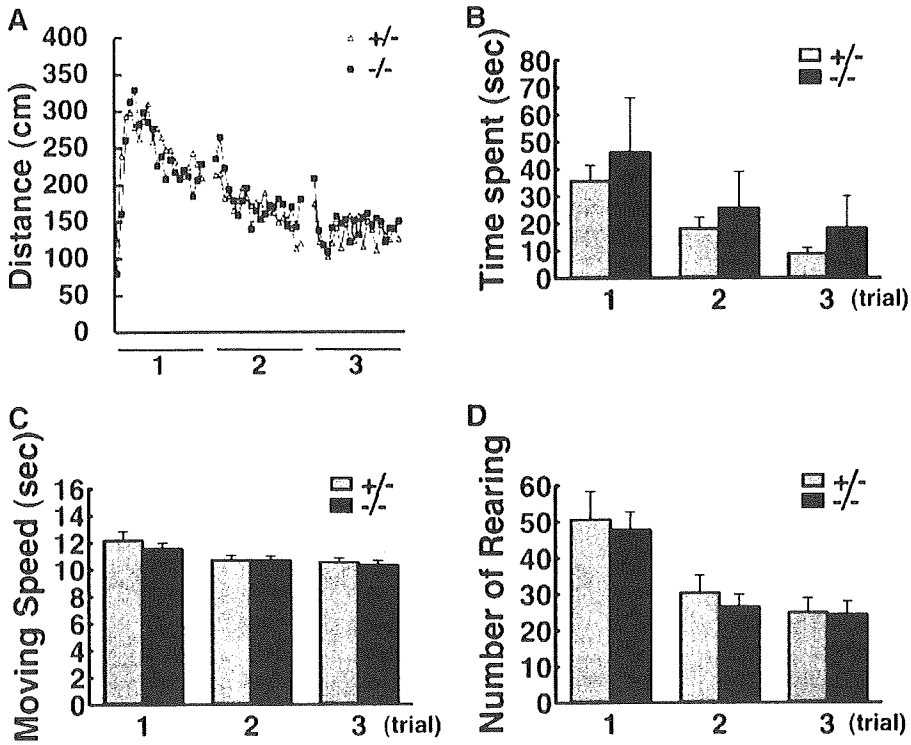


FIGURE 6. **Open field test.** Spontaneous activity in the open field test. *A*, distance moved every 30 s gradually decreased for both the β4GalT-II$^{+/-}$ and β4GalT-II$^{-/-}$ mice. *B*, time spent in the central area of the test chamber was slightly greater in the β4GalT-II$^{-/-}$ mice. The mean moving speed (*C*) and number of rearing (*D*) were not different between the genotypes. The spontaneous activity was suppressed normally in the initial phase of trial 1.

By Western blot analysis (Fig. 4*C*), we further confirmed that the HNK-1 carbohydrate in the β4GalT-II$^{-/-}$ mouse brain largely disappeared, except for faint bands of >250 kDa at every postnatal stage. On the other hand, the expression of NCAM, which is one of major carrier proteins of the HNK-1 carbohydrate, did not differ among the wild-type, β4GalT-II$^{+/-}$, and β4GalT-II$^{-/-}$ genotypes.

*Expression of PSA Is Not Changed in the β4GalT-II$^{-/-}$ Mouse Brain*—Immunohistochemical staining with an anti-PSA antibody showed that PSA was highly expressed in the hippocampus and corpus callosum and at lower levels in the cerebral cortex and cerebellar lobule of the 2-week-old β4GalT-II$^{+/+}$ mouse brain (Fig. 5*A*). Weak PSA expression was detected in the DG and CA3 fields of the hippocampus of the 11-week-old β4GalT-II$^{+/+}$ mouse (Fig. 5*B*). No obvious change in PSA expression was observed in the β4GalT-II$^{-/-}$ brain (Fig. 5, *A* and *B*). The comparable PSA expression in the mutant was verified by Western blot analysis (Fig. 5*C*) using the P0 mouse brain. The expression of NCAM also did not differ among the wild-type, β4GalT-II$^{+/-}$, and β4GalT-II$^{-/-}$ genotypes (Fig. 5*C*).

To examine the carbohydrate structures in the β4GalT-II$^{-/-}$ brain, lectin blot analysis using concanavalin A, RCA120, *S. sieboldiana* agglutinin, and *M. amurensis* agglutinin was performed. Although a few bands disappeared in the membrane fractions of the β4GalT-II$^{-/-}$ brain, most of the band patterns in the β4GalT-II$^{+/+}$ and β4GalT-II$^{-/-}$ brains of 2- and 11-week-old mice were comparable (supplemental Fig. 1).

*Spontaneous Activity of β4GalT-II$^{-/-}$ Mice in the Open Field Test*—To assess their spontaneous activity in a novel environment, the mice were subjected to an open field test for 3 days. Their spontaneous activity was typically and usually repressed at the initial phase of day 1 (Fig. 6*A*), probably because the animals became nervous in a novel environment. On every trial day, the greatest distance moved was recorded during the first phase of the trial (except for day 1), and this activity gradually decreased. This behavioral pattern did not significantly differ between the β4GalT-II$^{+/-}$ and β4GalT-II$^{-/-}$ mice. The β4GalT-II$^{-/-}$ mice also showed similar spontaneous activity in terms of their speed (Fig. 6*C*) and the number of rearing (Fig. 6*D*) as their heterozygous littermates, although the time spent in the central area of the chamber was slightly greater for the β4GalT-II$^{-/-}$ mice (Fig. 6*B*).

*Performance of β4GalT-II$^{-/-}$ Mice Is Impaired in the Morris Water Maze but Not in the Passive Avoidance Response Test*—In the Morris water maze paradigm, the swimming latency gradually decreased with the number of training trials and days for both the β4GalT-II$^{+/-}$ and β4GalT-II$^{-/-}$ mice (Fig. 7*A*). In the late phase of training, especially after day 6, the β4GalT-II$^{-/-}$ mice showed a significantly prolonged escape latency compared with the β4GalT-II$^{+/-}$ mice. We also observed that β4GalT-II$^{-/-}$ mice tended to swim near the pool wall (Fig. 7*C*, statistically not significant) with a particular swimming path (Fig. 7*B*). The swimming latency of the two genotypes was not different in visible landmark trials (Fig. 7*A*, +/−, 6.02 ± 0.48 s; −/−, 7.16 ± 0.72 s; $p = 0.38$), suggesting that swimming ability was normal in β4GalT-II$^{-/-}$ mice. On the other hand, in the passive avoidance response, another learning/memory paradigm, the β4GalT-II$^{-/-}$ mice performed the same as the +/− mice in a retention trial given 24 h after the electrical shock trial (Fig. 7*D*).

*β4GalT-II$^{-/-}$ Mice Show Motor Learning Retardation with Impaired Motor Coordination but GlcAT-P$^{-/-}$ Mice Do Not*—Motor function was assessed by the rota-rod and balance beam tests. Rota-rod performance, in which the latency to fall from the rod was measured, improved across trials and days for both the β4GalT-II$^{-/-}$ and β4GalT-II$^{+/-}$ mice (Fig. 8*A*). However, although the β4GalT-II$^{-/-}$ mice showed improved motor learning, their performance was always poorer than that of the β4GalT-II$^{+/-}$ mice. A relatively poor motor performance by the β4GalT-II$^{-/-}$ mice was also revealed by the balance beam test, in which a significantly greater number of hind foot slip-offs on the narrow (11 mm diameter) beam was observed

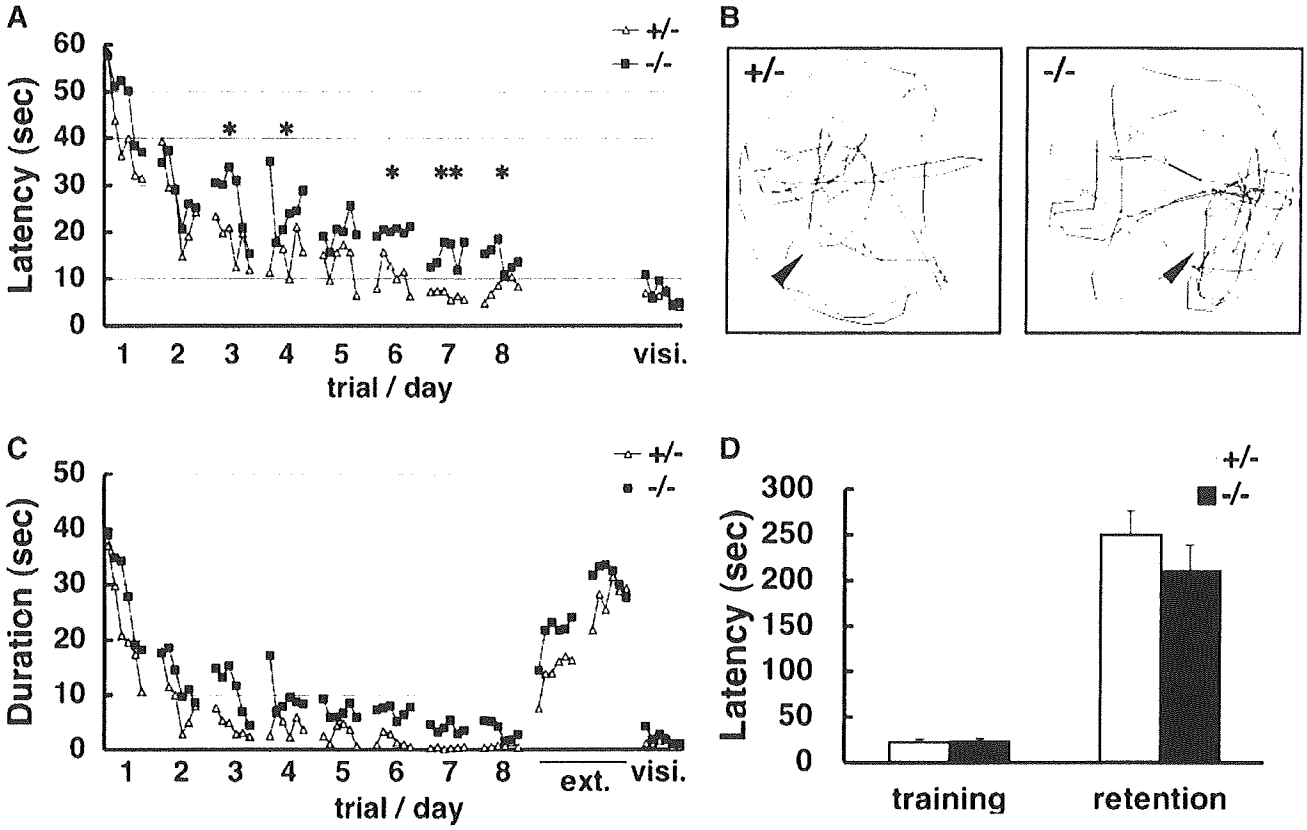


FIGURE 7. **Learning/memory performance in the Morris water maze task and passive avoidance.** *A*, swimming latency to reach the escape platform. The latency of the β4GalT-II$^{-/-}$ mice was significantly prolonged. *Asterisks* indicate a significant effect of genotype in each trial, by one-way analysis of variance (*, $p < 0.05$; **, $p < 0.01$). *B*, an example of a swimming path in the probe test without an escape platform. The β4GalT-II$^{-/-}$ mice tended to swim near the wall (at a distance from the platform). The *arrowhead* indicates the former location of the escape platform. *C*, swimming duration near the pool wall (10 cm from the wall). *ext.*, extinction trials (without platform); *visi.*, trial with a visible landmark on the platform. *D*, passive avoidance response was appropriately formed in both genotypes.

(Fig. 8*B*). In contrast, the hind paw movement of the β4GalT-II$^{-/-}$ mice was not impaired in a low speed rota-rod paradigm (7 rpm), as shown in Fig. 8*C*.

To clarify whether GlcAT-P$^{-/-}$ mice also had impaired motor function, these mice were subjected to the same tests. Unlike in the Morris water maze, the GlcAT-P$^{-/-}$ mice showed the same performance in both the rota-rod and balance beam tests as the GlcAT-P$^{+/+}$ mice (Fig. 8, *D* and *E*).

## DISCUSSION

In this study, we generated the first β4GalT-II$^{-/-}$ mice and analyzed their behavior, the histology, and immunohistochemical characteristics of their central nervous system. The β4GalT-II$^{-/-}$ mice grew normally and were fertile with no overt phenotypes, probably because β4GalT-I could compensate for the β4GalT activity in most tissues. However, spatial learning/memory and motor coordination/learning as well as the expression of the HNK-1 carbohydrate in the brain, where β4GalT-I is barely expressed, were severely impaired in the β4GalT-II$^{-/-}$ mice. Surprisingly, the amount of HNK-1 carbohydrate was markedly decreased in the cerebral cortex and hippocampus, moderately decreased in the cerebellar lobules, and unchanged in the cerebellar nuclei of the β4GalT-II$^{-/-}$ mice compared with their β4GalT-II$^{+/+}$ littermates. In Western blot analysis of whole-brain lysates, the HNK-1 carbohydrate was barely detectable in the β4GalT-II$^{-/-}$ mice, except as >250-kDa bands, although the NCAM expression was unchanged. The HNK-1 carbohydrate is mostly expressed on the Galβ1–4GlcNAc backbone, which can be synthesized by some β4GalTs. Our results indicate that β4GalT-II is indispensable for the expression of the HNK-1 carbohydrate in the brain. It is possible that β4GalT-II is solely responsible for the synthesis of Galβ1–4GlcNAc in the brain, even though β4GalT-III and -V are also expressed there (10, 13, 14). However, this is unlikely because RCA120-reactive bands, corresponding to Galβ1–4GlcNAc, were detected in the β4GalT-II$^{-/-}$ brain lysates at levels comparable with those in wild-type brain lysates (supplemental Fig. 1). Another possibility is that only the Galβ1–4GlcNAc that is synthesized by β4GalT-II can serve as a substrate for the HNK-1 carbohydrate, because of an unknown mechanism. In contrast, PSA expression in the brain was not affected in the β4GalT-II$^{-/-}$ mice, suggesting that β4GalT-II is dispensable for PSA expression. It is interesting that NCAM is glycosylated normally with PSA, but much less glycosylated with the HNK-1 carbohydrate in the β4GalT-II$^{-/-}$ mice, although NCAM is known to be modified with both carbohydrates. Among six putative *N*-glycosylation sites on NCAM,

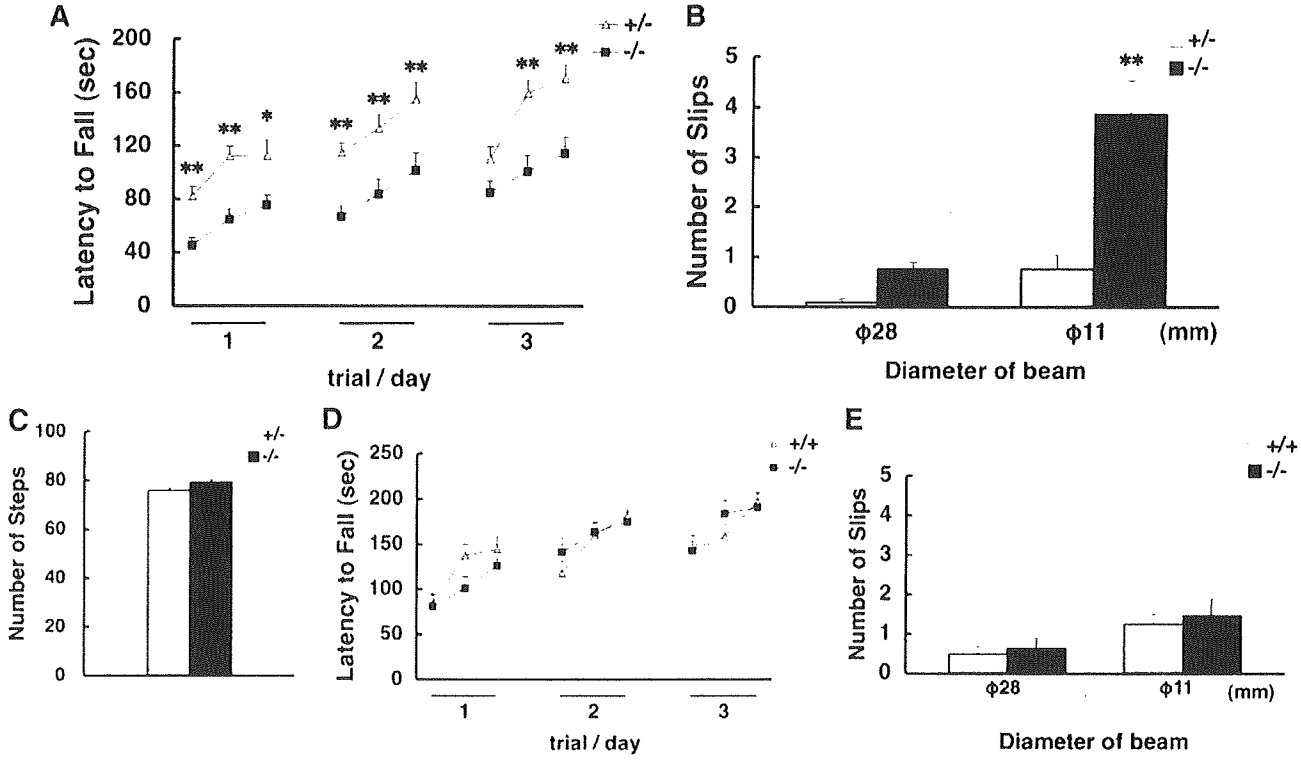


FIGURE 8. **Rota-rod and balance beam tests.** *A*, motor learning was consistently retarded in β4GalT-II $^{-/-}$ mice in the accelerating (5–40 rpm) rota-rod paradigm. *B*, in the balance beam test, the β4GalT-II$^{-/-}$ mice showed an increased number of hind limb slip offs compared with the β4GalT-II$^{+/-}$ mice (**, $p <$ 0.01; *t* test). *C*, number of hind limb steps was not different between the two genotypes in a low speed rota-rod test (7 rpm). *D*, rota-rod performance; *E*, balance beam test in GlcAT-P deficient mice. Their motor coordination was not impaired.

two of them (Asn-441 and Asn-470) and four of them (Asn-297, Asn-329, Asn-441, and Asn-470) could be modified by PSA and the HNK-1 carbohydrate, respectively (29). Our results suggest that β4GalT-II and other β4GalTs are responsible for the synthesis of *N*-glycans with the HNK-1 carbohydrate and *N*-glycans with PSA, respectively. If each β4GalT discriminates *N*-glycosylation sites on the same protein, it will be interesting.

The spontaneous activity of β4GalT-II$^{-/-}$ mice in a novel environment, assessed by the open field test, was comparable with that of control mice. Our results indicated that the β4GalT-II$^{-/-}$ mice had normal locomotor activity and could habituate to a novel environment with improvement seen in a single day and across days. In contrast, the performance of the β4GalT-II$^{-/-}$ mice in the Morris water maze was inferior to that of the controls. Taking into account their normal spontaneous activities in the open field situation, normal paw movement in the low speed rota-rod paradigm, and the same escape latency in the visible landmark water maze paradigm, impaired Morris water maze performance indicates impaired spatial learning/memory but not motor deficit in β4GalT-II$^{-/-}$ mice. In contrast, β4GalT-II$^{-/-}$ mice formed an appropriate passive response, another hippocampus-dependent paradigm, as well as the control mice. Thus, their learning/memory impairment was specific for spatial information processing and was not a broad spectrum learning/memory impairment.

There are previous findings showing the importance of HNK-1 carbohydrate and HNK-1-dependent relief in the hippocampal synaptic plasticity (30–32) and hippocampus-dependent learning/memory (33, 34). We and others expanded these previous studies using the mice deficient in GlcAT-P and HNK-1 sulfotransferase, which are responsible for glucuronic acid transfer and sulfate group transfer of the HNK-1 carbohydrate, respectively. These mutant mice exhibit a spatial learning/memory defect, as evaluated by the Morris water maze task, and also show reduced long term potentiation at the Schaffer-collateral-CA1 synapses, indicating that the HNK-1 carbohydrate plays a pivotal role in the synaptic plasticity of the hippocampus (35, 36). Based on these previous reports, the impaired spatial learning/memory of the β4GalT-II$^{-/-}$ mice in this study can be accounted for by the reduced expression of the HNK-1 carbohydrate in the brain of the mice, especially in the hippocampus.

Neural cell adhesion molecules, including NCAM, L1, tenascin-R, and telencephalin, play important roles in neuronal generation, cell migration, axonal outgrowth, and synaptic plasticity, and their functions are regulated by glycosylation structures such as the HNK-1 carbohydrate and PSA. NCAM, one of the best characterized members of the Ig superfamily, and the functions of PSA on NCAM have been extensively examined using NCAM-, ST8SiaII-, and ST8SiaIV-deficient mice (37–39). Some neuronal functions are dependent on PSA, and some others depend on NCAM. ST8SiaII and ST8SiaIV double-deficient (PSA-deficient), but not NCAM-deficient mice, die as neonates; this lethality is because of abnormal homophilic binding of NCAM in the absence of the negatively charged PSA (40). Because the HNK-1 carbohydrate is also neg-

atively charged and expressed on NCAM, a similar mechanism might be at work in mice deficient in HNK-1 carbohydrate production.

Motor coordination/learning, evaluated by the rota-rod and balance beam tests, was also impaired in the β4GalT-II$^{-/-}$ mice. Although the β4GalT-II$^{-/-}$ mice showed improved performance in the rota-rod test during successive trials and days, the latency to fall was always shorter than that of the control mice. The hind paw movement of the β4GalT-II$^{-/-}$ mice in the 7-rpm rota-rod test was no different from that of the +/− mice, suggesting that their motor ability was normal, at least in this low speed paradigm. These results suggest that the β4GalT-II$^{-/-}$ mice had retarded motor learning that was based on impaired motor coordination, although they had normal paw movement. In contrast, the GlcAT-P$^{-/-}$ mice performed normally in the rota-rod and balance beam tests. Therefore, the impaired motor coordination/learning of the β4GalT-II$^{-/-}$ mice was independent of the HNK-1 carbohydrate, unlike the impairment in spatial learning/memory. Because the band patterns of lectin blot (supplemental Fig. 1) were slightly different between the β4GalT-II$^{+/+}$ and β4GalT-II$^{-/-}$ mice, carbohydrate structures of some proteins could be altered in the β4GalT-II$^{-/-}$ brains. Unknown functional carbohydrates other than the HNK-1 carbohydrate and PSA are likely to play an important role in motor coordination/learning.

Although the NeuN-positive mature neurons in the cerebellar granular cell layer and hippocampus and the Nestin-positive neural progenitor cells in the DG and rostral migratory stream near the olfactory bulb appeared normal, the Purkinje cells in the cerebellum of the β4GalT-II$^{-/-}$ mice showed abnormalities. The number of Purkinje cells in the cerebellum was significantly reduced, and their alignment was partially disturbed in these mutant mice. These abnormalities in the Purkinje cells might be responsible for the impaired motor coordination/learning of the β4GalT-II$^{-/-}$ mice. Unknown functional carbohydrates synthesized by β4GalT-II could be involved in the development and maintenance of Purkinje cells.

The brain weight of the β4GalT-II$^{-/-}$ mice became significantly reduced at 6–9 months old, and the cerebral cortex showed slight atrophy at 8 months old. Because the present behavioral analysis was performed when the mice were between 3 and 6 months old, the reduction of brain size might occur during the behavioral tests. It is, however, unclear whether reduced brain size affected the behavioral performance of the β4GalT-II$^{-/-}$ mice. Previous studies reported that NCAM modified by PSA and PSA itself are important in cellular migration/lamination in the cerebral cortex and in the differentiation of neural precursors (41). However, neither PSA expression nor BrdUrd incorporation was altered in the brain of the β4GalT-II$^{-/-}$ mice in this study. Another possibility is that other adhesion molecules, which could be glycosylated, have key roles in brain formation and behavioral output. For example, mutations in the human L1 gene cause a severe neurological disease termed CRASH (acronym for corpus callosum hypoplasia, retardation, adducted thumbs, spastic paraplegia, and hydrocephalus) (42) and mouse mutations in the L1 gene also develop malformations of the nervous system (43, 44). Although the severity of brain malformations of L1$^{-/-}$ mice is different depending on genetic background, L1$^{-/-}$ mice with milder phenotypes display dilated lateral ventricles and reduced brain size as well as impaired Morris water maze performance (44). It might be possible that aberrant glycosylation of L1 changes L1 functions, resulting in dilated lateral ventricles and reduced brain size in β4GalT-II$^{-/-}$ mice. Further *in vivo* and *in vitro* analyses will be needed to address this issue.

In summary, the expression of the HNK-1 carbohydrate was markedly reduced in the brain of β4GalT-II$^{-/-}$ mice, suggesting that the expression of the HNK-1 carbohydrate, but not of PSA, was dependent on β4GalT-II. β4GalT-II$^{-/-}$ mice were impaired in spatial learning/memory and motor coordination/learning, indicating that carbohydrates synthesized by β4GalT-II play important roles in these higher brain functions. The spatial learning/memory could be dependent on the HNK-1 carbohydrate, but the motor coordination/learning was independent of it. Further investigation will be necessary to elucidate the roles of these and other carbohydrates in higher brain functions.

*Acknowledgments—We thank all the members of the Division of Transgenic Animal Science for excellent animal care.*

## REFERENCES

1. Kleene, R., and Schachner, M. (2004) *Nat. Rev. Neurosci.* **5,** 195–208
2. Asano, M., Furukawa, K., Kido, M., Matsumoto, S., Umesaki, Y., Kochibe, N., and Iwakura, Y. (1997) *EMBO J.* **16,** 1850–1857
3. Lu, Q., Hasty, P., and Shur, B. D. (1997) *Dev. Biol.* **181,** 257–267
4. Kumagai, T., Tanaka, M., Yokoyama, M., Sato, T., Shinkai, T., and Furukawa, K. (2009) *Biochem. Biophys. Res. Commun.* **379,** 456–459
5. Togayachi, A., Kozono, Y., Ishida, H., Abe, S., Suzuki, N., Tsunoda, Y., Hagiwara, K., Kuno, A., Ohkura, T., Sato, N., Sato, T., Hirabayashi, J., Ikehara, Y., Tachibana, K., and Narimatsu, H. (2007) *Proc. Natl. Acad. Sci. U. S. A.* **104,** 15829–15834
6. Mitoma, J., Bao, X., Petryanik, B., Schaerli, P., Gauguet, J. M., Yu, S. Y., Kawashima, H., Saito, H., Ohtsubo, K., Marth, J. D., Khoo, K. H., von Andrian, U. H., Lowe, J. B., and Fukuda, M. (2007) *Nat. Immunol.* **8,** 409–418
7. Biellmann, F., Hulsmeier, A. J., Zhou, D., Cinelli, P., and Hennet, T. (2008) *BMC Dev. Biol.* **8,** 109
8. Ellies, L. G., Tsuboi, S., Petryniak, B., Lowe, J. B., Fukuda, M., and Marth, J. D. (1998) *Immunity* **9,** 881–890
9. Henion, T. R., Raitcheva, D., Grosholz, R., Biellmann, F., Skarnes, W. C., Hennet, T., and Schwarting, G. A. (2005) *J. Neurosci.* **25,** 1894–1903
10. Lo, N. W., Shaper, J. H., Pevsner, J., and Shaper, N. L. (1998) *Glycobiology* **8,** 517–526
11. Hennet, T. (2002) *Cell. Mol. Life Sci.* **59,** 1081–1095
12. Almeida, R., Amado, M., David, L., Levery, S. B., Holmes, E. H., Merkx, G., van Kessel, A. G., Rygaard, E., Hassan, H., Bennett, E., and Clausen, H. (1997) *J. Biol. Chem.* **272,** 31979–31991
13. Nakamura, N., Yamakawa, N., Sato, T., Tojo, H., Tachi, C., and Furukawa, K. (2001) *J. Neurochem.* **76,** 29–38
14. Sasaki, N., Manya, H., Okubo, R., Kobayashi, K., Ishida, H., Toda, T., Endo, T., and Nishihara, S. (2005) *Biochem. Biophys. Res. Commun.* **333,** 131–137
15. Kido, M., Asano, M., Iwakura, Y., Ichinose, M., Miki, K., and Furukawa, K. (1998) *Biochem. Biophys. Res. Commun.* **245,** 860–864
16. Asano, M., Nakae, S., Kotani, N., Shirafuji, N., Nambu, A., Hashimoto, N., Kawashima, H., Hirose, M., Miyasaka, M., Takasaki, S., and Iwakura, Y. (2003) *Blood* **102,** 1678–1685
17. Mori, R., Kondo, T., Nishie, T., Ohshima, T., and Asano, M. (2004) *Am. J. Pathol.* **164,** 1303–1314
18. Nishie, T., Miyaishi, O., Azuma, H., Kameyama, A., Naruse, C., Hashi-

moto, N., Yokoyama, H., Narimatsu, H., Wada, T., and Asano, M. (2007) *Am. J. Pathol.* **170,** 447–456
19. Lu, Q., and Shur, B. D. (1997) *Development (Camb.)* **124,** 4121–4131
20. Soriano, P., Montgomery, C., Geske, R., and Bradley, A. (1991) *Cell* **64,** 693–702
21. Yagi, T., Nada, S., Watanabe, N., Tamemoto, H., Kohmura, N., Ikawa, Y., and Aizawa, S. (1993) *Anal. Biochem.* **214,** 77–86
22. Kuhn, R., Rajewsky, K., and Muller, W. (1991) *Science* **254,** 707–710
23. Nagy, A., Rossant, J., Nagy, R., Abramow-Newerly, W., and Roder, J. C. (1993) *Proc. Natl. Acad. Sci. U. S. A.* **90,** 8424–8428
24. Tagawa, H., Kizuka, Y., Ikeda, T., Itoh, S., Kawasaki, N., Kurihara, H., Onozato, M. L., Tojo, A., Sakai, T., Kawasaki, T., and Oka, S. (2005) *J. Biol. Chem.* **280,** 23876–23883
25. Paxinos, G., and Franklin, K. (2001) *The Mouse Brain in Stereotaxic Coordinates,* 2nd Ed., Academic Press, San Diego
26. Morris, R. G., Garrud, P., Rawlins, J. N., and O'Keefe, J. (1982) *Nature* **297,** 681–683
27. Barlow, C., Hirotsune, S., Paylor, R., Liyanage, M., Eckhaus, M., Collins, F., Shiloh, Y., Crawley, J. N., Ried, T., Tagle, D., and Wynshaw-Boris, A. (1996) *Cell* **86,** 159–171
28. Carter, R. J., Morton, J., and Dunnett, S. B. (2003) *Current Protocols in Neuroscience,* pp. 8.12.1–8.12.14, Wiley-Liss, Hoboken, NJ
29. Liedtke, S., Geyer, H., Wuhrer, M., Geyer, R., Frank, G., Gerardy-Schahn, R., Zahringer, U., and Schachner, M. (2001) *Glycobiology* **11,** 373–384
30. Saghatelyan, A. K., Gorissen, S., Albert, M., Hertlein, B., Schachner, M., and Dityatev, A. (2000) *Eur. J. Neurosci.* **12,** 3331–3342
31. Saghatelyan, A. K., Snapyan, M., Gorissen, S., Meigel, L., Mosbacher, J., Kaupmann, K., Bettler, B., Kornilov, A. V., Nifantiev, N. E., Sakanyan, V., Schachner, M., and Dityatev, A. (2003) *Mol. Cell. Neurosci.* **24,** 271–282
32. Bukalo, O., Fentrop, N., Lee, A. Y., Salmen, B., Law, J. W., Wotjak, C. T., Schweizer, M., Dityatev, A., and Schachner, M. (2004) *J. Neurosci.* **24,** 1565–1577
33. Bukalo, O., Schachner, M., and Dityatev, A. (2007) *J. Neurosci.* **27,** 6019–6028
34. Strekalova, T., Wotjak, C. T., and Schachner, M. (2001) *Mol. Cell. Neurosci.* **17,** 1102–1113
35. Senn, C., Kutsche, M., Saghatelyan, A., Bosl, M. R., Lohler, J., Bartsch, U., Morellini, F., and Schachner, M. (2002) *Mol. Cell. Neurosci.* **20,** 712–729
36. Yamamoto, S., Oka, S., Inoue, M., Shimuta, M., Manabe, T., Takahashi, H., Miyamoto, M., Asano, M., Sakagami, J., Sudo, K., Iwakura, Y., Ono, K., and Kawasaki, T. (2002) *J. Biol. Chem.* **277,** 27227–27231
37. Eckhardt, M., Bukalo, O., Chazal, G., Wang, L., Goridis, C., Schachner, M., Gerardy-Schahn, R., Cremer, H., and Dityatev, A. (2000) *J. Neurosci.* **20,** 5234–5244
38. Angata, K., Long, J. M., Bukalo, O., Lee, W., Dityatev, A., Wynshaw-Boris, A., Schachner, M., Fukuda, M., and Marth, J. D. (2004) *J. Biol. Chem.* **279,** 32603–32613
39. Hildebrandt, H., Muhlenhoff, M., Weinhold, B., and Gerardy-Schahn, R. (2007) *J. Neurochem.* **103,** Suppl. 1, 56–64
40. Weinhold, B., Seidenfaden, R., Rockle, I., Muhlenhoff, M., Schertzinger, F., Conzelmann, S., Marth, J. D., Gerardy-Schahn, R., and Hildebrandt, H. (2005) *J. Biol. Chem.* **280,** 42971–42977
41. Angata, K., Huckaby, V., Ranscht, B., Terskikh, A., Marth, J. D., and Fukuda, M. (2007) *Mol. Cell. Biol.* **27,** 6659–6668
42. Fransen, E., Lemmon, V., Van Camp, G., Vits, L., Coucke, P., and Willems, P. J. (1995) *Eur. J. Hum. Genet.* **3,** 273–284
43. Dahme, M., Bartsch, U., Martini, R., Anliker, B., Schachner, M., and Mantei, N. (1997) *Nat. Genet.* **17,** 346–349
44. Fransen, E., D'Hooge, R., Van Camp, G., Verhoye, M., Sijbers, J., Reyniers, E., Soriano, P., Kamiguchi, H., Willemsen, R., Koekkoek, S. K., De Zeeuw, C. I., De Deyn, P. P., Van der Linden, A., Lemmon, V., Kooy, R. F., and Willems, P. J. (1998) *Hum. Mol. Genet.* **7,** 999–1009

THE JOURNAL OF BIOLOGICAL CHEMISTRY VOL. 284, NO. 14, pp. 9247–9256, April 3, 2009


# Distinct Transport and Intracellular Activities of Two GlcAT-P Isoforms*[S]

Received for publication, September 29, 2008, and in revised form, December 17, 2008 Published, JBC Papers in Press, January 30, 2009, DOI 10.1074/jbc.M807517200

Yasuhiko Kizuka[‡], Yasuhiro Tonoyama[§], and Shogo Oka[§1]

*From the [‡]Department of Biological Chemistry, Graduate School of Pharmaceutical Sciences, and the [§]Department of Biological Chemistry, Human Health Sciences, Graduate School of Medicine, Kyoto University, Kyoto 606-8507, Japan*

**A neural glycotope, human natural killer-1 carbohydrate, is involved in synaptic plasticity. The key biosynthetic enzyme is a glucuronyltransferase, GlcAT-P, a type II membrane protein comprising an N-terminal cytoplasmic tail, transmembrane domain, stem region, and C-terminal catalytic domain. Previously, we reported that GlcAT-P has two isoforms differing in only the presence or absence of the N-terminal 13 amino acids (P-N13) in the cytoplasmic tail, but the functional distinction of these two isoforms has not been reported. Herein, we show that when expressed in Neuro2A cells, short form GlcAT-P (sGlcAT-P) exhibited significantly higher glucuronylation activity than the longer form (lGlcAT-P), despite their comparable specific activities *in vitro*. In addition, sGlcAT-P was strictly localized in Golgi apparatus, whereas lGlcAT-P was mainly localized in Golgi but partly in the endoplasmic reticulum. We demonstrated that the small GTPase, Sar1, recognized a dibasic motif in the cytoplasmic tail near P-N13 that was important for exiting the endoplasmic reticulum, and Sar1 interacted with sGlcAT-P more strongly than lGlcAT-P. Finally, the attachment of P-N13 to another glycosyltransferase, polysialyltransferase-I (ST8Sia-IV), had similar effects, such as reduced activity and entrapment within endoplasmic reticulum. These results suggest that P-N13 can control glycosyltransferase transport through Sar1 binding interference.**

A number of reports have revealed that glycosylation plays diverse roles in many biological events, such as development and disease progression (1). During glycan biosynthesis, ER-[2] and Golgi-resident glycosyltransferases catalyze reactions in a stepwise manner to construct diverse glycoconjugates (2). Among glycan epitopes (glycotopes), we have been investigating the functions of human natural killer-1 (HNK-1) carbohydrate, which is highly expressed on several cell adhesion molecules in the nervous system (3). This carbohydrate epitope, comprising a unique trisaccharide structure, $HSO_3$-3GlcAβ1–3Galβ1–4GlcNAc-, is sequentially biosynthesized by one of two glucuronyltranferases (GlcAT-P and GlcAT-S) and by a specific sulfotransferase (HNK-1ST) (4–6). We generated and analyzed GlcAT-P gene-deficient mice and revealed that the marked loss of the HNK-1 carbohydrate in the nervous system caused the impairment of hippocampal synaptic plasticity, learning, and memory (7). These results indicated that GlcAT-P is the main HNK-1-synthesizing enzyme in the brain and that this carbohydrate is important to maintain proper neural function. Therefore, elucidation of the regulatory mechanism for the HNK-1 biosynthesis will lead to the clarification of how this carbohydrate controls neural function. Recently, we reported that an enzyme complex consisting of GlcAT-P (or GlcAT-S) and HNK-1ST positively regulates the efficiency of HNK-1 biosynthesis (8). In addition, it was reported that other glycosyltransferases and glycosylation-related proteins were associated in cells to regulate glycoconjugate biosynthesis (9). Therefore, it is evident that not only the expression of a glycosyltransferase but also its regulation mechanism, including enzyme complex formation, is indispensable to understand the overall glycosylation system *in vivo*.

Most glycosyltransferases are commonly type II membrane proteins, comprising a short N-terminal cytoplasmic tail, transmembrane domain, stem region, and large C-terminal catalytic domain (10). Most of them reside at a specific location in the Golgi apparatus (11), where specific glycosylation occurs. The currently supported concept is that the region comprising the N-terminal cytoplasmic tail to the stem domain is sufficient for the Golgi retention of glycosyltransferase and that the C-terminal domain is responsible for the catalytic reaction. In fact, some chimeric enzymes consisting of an N-terminal region (from the N terminus to stem) fused with a fluorescent protein like green fluorescent protein exhibited appropriate localization in the Golgi apparatus (12), whereas recombinant soluble catalytic domains showed enzymatic activities with high substrate specificities *in vitro* (13). In recent years, however, a growing number of findings have revealed that the N-terminal cytoplasmic tail of glycosyltransferases plays various roles in cells. For instance, β1,4-galactosyltransferase-I (B4GalT-I) has two forms differing in their cytoplasmic tail length, and it was shown that the longer form was localized both in the Golgi apparatus and on the cell surface, whereas the

* This work was supported in part by Grant-in-Aid for Creative Scientific Research 16GS0313 (to S. O.) and a Grant-in-Aid for JSPS Fellows (to Y. K.) from the Ministry of Education, Culture, Sports, Science, and Technology. The costs of publication of this article were defrayed in part by the payment of page charges. This article must therefore be hereby marked "*advertisement*" in accordance with 18 U.S.C. Section 1734 solely to indicate this fact.

[S] The on-line version of this article (available at http://www.jbc.org) contains supplemental Fig. 1.

[1] To whom correspondence should be addressed: Kawahara-cho 53, Shogoin, Sakyo-ku, Kyoto 606-8507, Japan. Tel./Fax: 81-75-751-3959; E-mail: shogo@hs.med.kyoto-u.ac.jp.

[2] The abbreviations used are: ER, endoplasmic reticulum; B4GalT-I, β1,4-galactosyltransferase-I; GlcAT, glucuronyltransferase; G-N13, N-terminal 13 amino acids of long form B4GalT-I; HNK-1, human natural killer-1; lGlcAT-P, long form GlcAT-P; P-N13, N-terminal 13 amino acids of lGlcAT-P; PNGase F, peptide:*N*-glycosidase F; PSA, polysialic acid; PST, polysialyltransferase-I; sGlcAT-P, short form GlcAT-P; ST6Gal-I, β-galactoside α2,6-sialyltransferase-I; mAb, monoclonal antibody; pAb, polyclonal antibody.

shorter form resided only in the Golgi (14), and that the cycling between the *trans*-Golgi cisterna and the *trans*-Golgi network was mediated by a signal contained in the longer cytoplasmic tail (15). Maccioni's group (16) reported that the basic amino acid motifs commonly found in the cytoplasmic tails of some glycosyltransferases were required for their exit from ER to the Golgi apparatus. More recently, it was reported that Vps74p recognized and bound to the cytoplasmic tails of many glycosyltransferases and functioned to retain them in the Golgi apparatus in yeast (17, 18). These reports underscore the importance of the cytoplasmic tail of glycosyltransferases, especially for their appropriate localization in cells.

Previously, we reported that GlcAT-P mRNA has two alternative splicing variants in mouse, rat, and human brains (19, 20). A 16-bp insertion was found soon after the initiation codon in the longer mRNA in mice (20), and a similar 17-bp insertion was found in humans (19) (Fig. 1*A*). Since the insertion created a new stop codon in frame, the second ATG (Fig. 1*A*, *underlined*) was probably used as an alternative initiation codon. As a result, the longer mRNA was translated into a shorter protein. Therefore, the alternative splicing generates the long and short forms of the enzyme, and these two isoforms are considered to be identical except for the additional N-terminal 13 amino acids in the cytoplasmic tail (Fig. 1*B*, lGlcAT-P and sGlcAT-P). However, no functional difference between these two isoforms has yet been clarified. In this study, we found significant differences in intracellular activity and localization between the two isoforms, probably caused by the distinct rate of export from ER. These data suggest a unique Golgi localization mechanism of GlcAT-P involving the cytoplasmic tail.

## EXPERIMENTAL PROCEDURES

*Materials*—Monoclonal antibody (mAb) M6749 was a generous gift from Dr. H. Tanaka (Kumamoto University). Mouse anti-FLAG M2 mAb was purchased from Sigma. Rabbit anti-GlcAT-P pAb (GP2) was raised in a rabbit against the recombinant human GlcAT-P catalytic region expressed and purified from *Escherichia coli*. Rabbit anti-P-N13 (corresponding to the N-terminal 13 amino acids of lGlcAT-P) pAb was raised against a synthetic peptide (MGNEELWAQPALE). Mouse anti-PSA mAb (12E3) was kindly provided by Dr. T. Seki (Juntendo University). Mouse anti-T7 mAb was purchased from Novagen (Madison, WI). Mouse anti-GM130 mAb was purchased from BD Biosciences. Rabbit anti-human IgG-Fc pAb was from Jackson ImmunoResearch Laboratories (West Grove, PA). Biotinylated wheat germ agglutinin was from Seikagaku Corp. (Tokyo, Japan). Horseradish peroxidase-conjugated anti-mouse IgG, anti-mouse IgM, and anti-rabbit IgG were purchased from Zymed Laboratories Inc. (South San Francisco, CA). Alexa Fluor 488-conjugated anti-rabbit IgG and Alexa Fluor 546-conjugated anti-mouse IgG were obtained from Molecular Probes, Inc. (Eugene, OR). Rhodamine-conjugated Avidin D was from Vector Laboratories (Burlingame, CA). Protein G-Sepharose TM4 Fast Flow was purchased from GE Healthcare.

*Expression Plasmids*—The subcloning of rat lGlcAT-P cDNA into pEF-BOS (pEF-BOS/lGlcAT-P) was performed as described previously (4). Rat sGlcAT-P cDNA (including a 16-bp (GTGGGTGTGAGCGCTG) insertion right after the initiation codon for lGlcAT-P) was subcloned into pEF-BOS (pEF-BOS/sGlcAT-P) in the same way as for pEF-BOS/lGlcAT-P. The insertion of lGlcAT-PΔstem cDNA into pEF-1/V5-His A (Invitrogen) was performed as follows. Two fragments were amplified by PCR using pEF-BOS/lGlcAT-P as a template with the two sets of primers listed below to create a 5′-EcoRI site in the shorter fragment and a 3′-NotI site in the longer fragment. After the fragments had been digested with EcoRI or NotI, respectively, the ends of both fragments were phosphorylated with polynucleotide kinase. Then the two fragments were simultaneously ligated to pEF-1/V5-His A, which had been double-digested with EcoRI and NotI. The expression plasmid for lGlcAT-P-AAA (pEF-BOS/lGlcAT-P-AAA) was constructed using QuikChange Lightning site-directed mutagenesis kits (Stratagene, La Jolla, CA) according to the manufacturer's protocol employing the primers listed below, with pEF-BOS/lGlcAT-P being used as a template. GlcAT-P-Fc (P-long-Fc, P-short-Fc, and P-AAA-Fc) expression plasmids were constructed as follows. A fragment was amplified by PCR using pEF-BOS/lGlcAT-P, pEF-BOS/sGlcAT-P, or pEF-BOS/lGlcAT-P-AAA as a template with the primers listed below to create a 3′-SpeI site. After the resulting fragment had been digested with SpeI, it was ligated to pEF-Fc, which had been double-digested with EcoRV and SpeI. The G-N13-GlcAT-P expression plasmid was constructed as follows. A fragment was amplified by PCR using pEF-BOS/lGlcAT-P as a template with the primers listed below to create a 3′-NotI site. After the fragment had been digested with NotI, it was phosphorylated with polynucleotide kinase. An annealed oligonucleotide corresponding to human B4GalT-I N-terminal 13 amino acids with a 5′-EcoRI stub was prepared using the synthetic oligonucleotides listed below. These two fragments were simultaneously ligated to pEF1/V5-HisA, which had been double-digested with EcoRI and NotI. The expression plasmid for G-N13AA-GlcAT-P was constructed using QuikChange Lightning site-directed mutagenesis kits employing the primers listed below, with pEF-1/V5-HisA/G-N13-GlcAT-P being used as a template. cDNA of the mouse PST (ST8Sia-IV)-coding sequence was amplified by PCR with the primers listed below using reverse-transcribed mouse brain total RNA as a template to create 5′-HindIII and 3′-XbaI sites. The fragment was ligated to p3×FLAG-CMV-14 (Sigma), which had been double-digested with the same enzymes. Construction of the P-N13-PST and G-N13-PST expression plasmids was performed as follows. A fragment was amplified by PCR using the PST expression construct as a template with the primers listed below to create a 3′-XbaI site. After the fragment had been digested with XbaI, it was phosphorylated with polynucleotide kinase. An annealed oligonucleotide corresponding to the lGlcAT-P N-terminal 13 amino acids or those from human B4GalT-I with a 5′-HindIII stub was prepared using the synthetic oligonucleotides listed below. These two fragments were simultaneously ligated to p3×FLAG-CMV-14, which had been double-digested with HindIII and XbaI.

*Primers and Oligonucleotides*—Primers and nucleotides were listed as follows: lGlcAT-PΔstem for the longer fragment, TCCGACACGCTGCCCACCAT and TGAGCGGCCGCT-CAGATCTCCACCGAGGGGT (primer 1), for the shorter

fragment, CATGAATTCGGACTCTGCAAACCTGCTGC and GCTCTGGTGCCAGACGGTGA; lGlcAT-P-AAA, GGCGCAGCCAGCCTTGGAGATGCCGGCGGCAGCGGACATCCTCGCG and the complementary sequence; P-long-Fc and P-AAA-Fc, GCCACCATGGGTAATGAGGAGCTGTG and CCGACTAGTACTCACCCACCACCTCCACGATGTCAC (primer 2); P-short-Fc, GCCACCATGCCGAAGAGAAGGGACAT and primer 2; G-N13-GlcAT-P primers, ATGCCGAAGAGAAGGGACAT and primer 1; G-N13-GlcAT-P oligonucleotides, AATTGCCACCATGAGGCTTCGGGAGCCGCTCCTGAGCGGCAGCGCCGCG and CGCGGCGCTGCCGCTCAGGAGCGGCTCCCGAAGCCTCATGGTGGC (oligonucleotide 1); G-N13AA-GlcAT-P, GGTGGAATTGCCACCATGGCGCTTGCGGAGCCGCTCCTGAGCGGC and the complementary sequence; PST, TTTAAGCTTCACCCAAGATGCGCTCAATT and TGTTCTAGATTGCTTCATGCACTTTCCTG (primer 3); P-N13-PST primers, ATGCGCTCAATTAGAAAACG and primer 3, oligonucleotides, AGCTGCCACCATGGGTAATGAGGAGCTGTGGGCGCAGCCAGCCTTGGAG and CTCCAAGGCTGGCTGCGCCCACAGCTCCTCATTACCCATGGTGGC; G-N13-PST oligonucleotides, AGCTGCCACCATGAGGCTTCGGGAGCCGCTCCTGAGCGGCAGCGCCGCG and oligonucleotide 1. Underlining indicates restriction sites.

*Cell Culture and Transfection*—Neuro2A cells were cultured in minimum Eagle's medium supplemented with Earle's salts, nonessential amino acids, and 10% fetal bovine serum. For transfection, cells, plated on 6-cm (or 10-cm) tissue culture dishes, were transfected with 1 $\mu$g (4 $\mu$g in the case of 10-cm dishes) of each expression vector using FUGENE6 transfection reagent (Roche Applied Science) according to the manufacturer's protocol. After a 6-h incubation, the culture medium was replaced with serum-free Opti-MEM I (Invitrogen) in the case of analyzing proteins secreted into the medium. Cells and media were collected at 24 h post-transfection. The collected culture medium was ultracentrifuged at 105,000 $\times$ *g* for 20 min to exclude contamination by cellular membranous components, and proteins secreted into the culture medium were precipitated with ethanol and then solubilized in Laemmli sample buffer.

*SDS-PAGE and Western Blotting*—SDS-PAGE and Western blotting were carried out as described previously (8). In the case of PSA detection, 2% BSA in PBS containing 0.05% Tween 20 was used for blocking and antibody dilution. For the other antibodies, 5% skim milk in PBS containing 0.05% Tween 20 was used. Protein bands were detected with SuperSignal West Pico (Pierce) using a Luminoimage Analyzer LAS-3000 (Fuji Film, Tokyo, Japan).

*N-Glycosidase F Digestion*—Proteins (50 $\mu$g) were denatured with PBS containing 0.5% SDS, 1% 2-mercaptoethanol, and 4 mM EDTA. After the solution had been diluted with 4 volumes of PBS containing Nonidet P-40 (final concentration, 0.5%), 5 units of *N*-glycosidase F (Roche Applied Science) was added, followed by incubation for 12 h at 37 °C.

*Immunofluorescence Staining*—At 24 h post-transfection, cells were washed with PBS, fixed with ice-cold methanol, and then incubated with primary antibodies followed by incubation with Alexa Fluor-conjugated secondary antibodies. For DsRed2 detection, cells were fixed at 48 h post-transfection with 4% paraformaldehyde in PBS and blocked with 3% bovine serum albumin in PBS containing 0.1% Triton X-100. Cells were visualized with a Fluoview laser confocal microscope system (Olympus, Tokyo, Japan).

*Glucuronyltransferase Assay*—Glucuronyltransferase activity toward asialo-orosomucoid was measured as described previously (8). As an enzyme source, a Neuro2A cell lysate or concentrated conditioned medium was prepared. Neuro2A cells were plated on 10-cm culture dishes and then transfected with the expression plasmid, followed by medium replacement with Opti-MEM I after a 6-h incubation. Cells were collected at 48 h after transfection and lysed with 500 $\mu$l of Tris-buffered saline containing 1% Triton X-100 and a protease inhibitor mixture (Nacalai Tesque, Kyoto, Japan), and after centrifugation, the clarified lysate was used. The culture medium was ultracentrifuged, as described above, and then used after concentration to 500 $\mu$l with an Amicon Ultra centrifugal filter device (Millipore, Bedford, MA). 5 $\mu$l of each solution was used as an enzyme source.

*Co-precipitation Experiment*—We performed a co-precipitation experiment in which we referred to a method used in an *in vitro* binding experiment between Sar1 and immobilized cytoplasmic tail peptides of glycosyltransferases (16). Human recombinant full-length Sar1 protein fused to T7 tag at its N terminus was purchased from Abcam (Cambridge, MA). Neuro2A cells, plated on 6-cm culture dishes, were transfected with the expression plasmid encoding P-long-Fc, P-short-Fc, or P-AAA-Fc and then lysed with 300 $\mu$l of Tris-buffered saline containing 1% Triton X-100 and protease inhibitors. After centrifugation at 15,000 $\times$ *g* for 10 min, 1.2 $\mu$g of T7-tagged Sar1 was added to the supernatant, and then the mixture was incubated for 30 min at 4 °C. A fraction of the mixture was recovered for Western blotting, with Protein G-Sepharose TM4 Fast Flow being added to the rest of the mixture, followed by incubation for 2 h. The beads were precipitated and washed three times with an excess volume of the buffer (Tris-buffered saline containing 0.5% Triton X-100). Proteins bound to the beads were eluted by boiling in Laemmli sample buffer.

## RESULTS

*Enhanced N-Glycan Glucuronylation by sGlcAT-P in Neuro2A Cells*—Previously, we reported that GlcAT-P mRNA had two alternatively spliced variants in mouse, rat, and human brains (19, 20). As described above, a 16-bp insertion in mice or a 17-bp insertion in humans in the longer mRNA generated a new stop codon in-frame (Fig. 1*A*). As a result, longer mRNAs containing the insertion were translated to the short form proteins and *vice versa*, and the long and short enzymes differed in only the presence or absence of the N-terminal 13 amino acids (P-N13) in the cytoplasmic tail (Fig. 2*A*, lGlcAT-P and sGlcAT-P). We subcloned the rat cDNAs complementary to the two forms of mRNA using a rat brain cDNA pool and confirmed that a similar 16-bp insertion was also present in rats (Fig. 1*A*). To investigate the respective role of these two protein isoforms in cells, rat cDNAs (lGlcAT-P cDNA and sGlcAT-P cDNA complementary to the shorter and longer mRNA, respectively) were transfected into the neuroblastoma cell line Neuro2A.

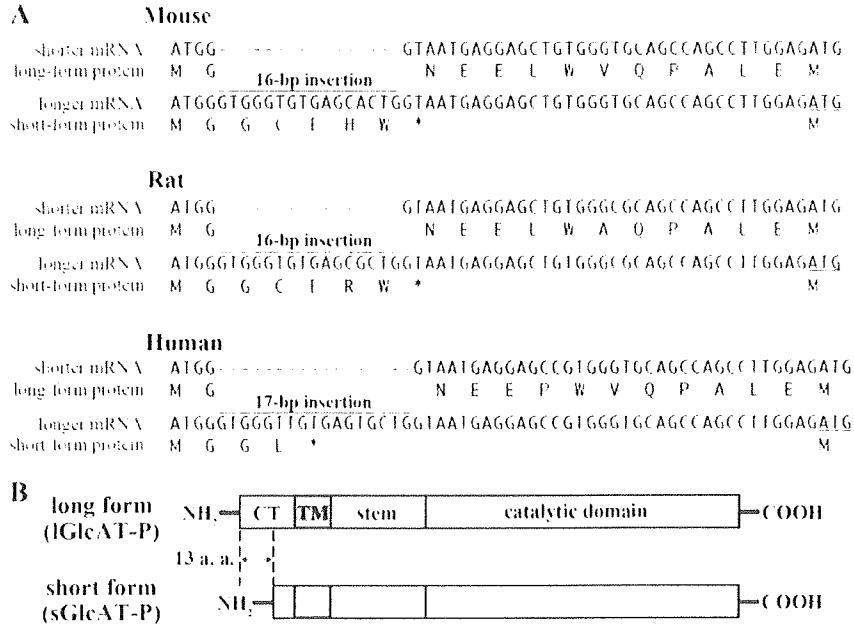


FIGURE 1. **Spliced variants of GlcAT-P.** *A*, cDNA sequences are shown around the initiation ATG complementary to the shorter and longer mRNA forms in mice, rats, and humans, and the corresponding amino acid sequence is depicted just *under* the respective cDNA sequence. The *underlined ATG* is a presumed initiation codon used in the longer mRNA. *B*, schematic diagram of lGlcAT-P and sGlcAT-P proteins. *CT*, cytoplasmic tail. *TM*, transmembrane domain.

After the cells had been harvested and lysed, they were treated with peptide:*N*-glycosidase F (PNGase F) to remove *N*-glycans to show the enzyme expression level clearly and then subjected to Western blotting (Fig. 2*B*). GP2 is an anti-GlcAT-P pAb against the GlcAT-P catalytic domain, which showed that almost equivalent amounts of the long and short isoforms were expressed (Fig. 2*B*, *top right*). In addition, only lGlcAT-P was detected with anti-P-N13, which is a rabbit pAb recognizing P-N13 (Fig. 2*B*, *bottom right panel*). To confirm that the second ATG was actually used as a translation initiation site when sGlcAT-P cDNA was transfected, we also subcloned GlcAT-P cDNA starting from the second ATG (Fig. 1*A*, *underlined*) integrated just downstream of an artificial Kozak sequence, GCCACC, into an expression vector, pEF1/V5-His A. The transfection of this construct into Neuro2A cells resulted in the same enzyme expression as in the case of sGlcAT-P cDNA regarding the molecular weight, biosynthetic activity, and subcellular localization (data not shown), indicating that in sGlcAT-P cDNA, including the 16-bp insertion, the second ATG was actually used as an initiation codon. Therefore, we employed sGlcAT-P cDNA in subsequent experiments. M6749 mAb, which exhibits similar epitope specificity to HNK-1 mAb, reacts with the HNK-1 epitope regardless of the terminal sulfate group (21). Since no band was detected for mock-transfected Neuro2A cells with M6749 mAb, Western blotting with this antibody allowed us to determine the amount of carbohydrate antigen synthesized by GlcAT-P expressed in the cells (Fig. 2*B*, *left*). As a result, a significantly higher expression level of the M6749 epitope on *N*-glycan was found in sGlcAT-P-expressing cells than in lGlcAT-P-expressing ones, despite the almost equivalent expression levels of the two enzymes. This indicates that sGlcAT-P has the ability to biosynthesize more abundant HNK-1 epitopes in cells than lGlcAT-P. It is possible that this higher epitope production was caused by the higher specific activity of sGlcAT-P, so we performed an *in vitro* activity assay using a Neuro2A cell lysate to compare the specific activities of the two GlcAT-P isoforms (Fig. 2*C*). Western blotting of the enzyme source extracts used for the activity assay (Fig. 2*C*, *right*) showed comparable enzyme expression and distinct product expression consistent with the results in Fig. 2*B*. However, the specific activities toward a glycoprotein acceptor substrate of the two isoforms were comparable (Fig. 2*C*, *left*), reflecting the enzyme expression levels. This excluded the possibility that the higher product biosynthesis in sGlcAT-P-expressing cells was due to its higher specific activity.

*Subcellular Localization and Secretion of the Two GlcAT-P Isoforms*—Next, we investigated the subcellular localization of the two GlcAT-P isoforms. Neuro2A cells expressing lGlcAT-P or sGlcAT-P were immunostained with GP2 pAb and anti-GM130 mAb (Golgi marker) (Fig. 3*A*). As a result, sGlcAT-P was found to show strict accumulation in the Golgi apparatus, whereas lGlcAT-P was localized mainly in the Golgi but partly in the ER (Figs. 3*A* and 4*B*), suggesting that some lGlcAT-P remained in the ER, probably due to slow export from the ER. The results were similar to the two isoforms of a sialyltransferase, ST6Gal-I (22). The two isoforms of this enzyme differ in only a single amino acid in the catalytic domain generated on RNA editing. The ST6Gal-I isoforms were differently localized in cells like those of GlcAT-P (23). ST6Gal-I is well known to be cleaved at its stem region and secreted extracellularly as a soluble form (24), and the secretion levels of the two isoforms were shown to significantly differ (23). Based on these reports, we investigated whether or not GlcAT-P was cleaved and secreted (Fig. 3*B*). As a result, two bands were detected for both lGlcAT-P- and sGlcAT-P-expressing cell media, and the cleavage and secretion level of sGlcAT-P were higher than those of lGlcAT-P. The *in vitro* activity assay also confirmed the higher secretion of sGlcAT-P (Fig. 3*C*) and indicated that the cleaved GlcAT-P was catalytically active with an intact catalytic domain. Since many secreted glycosyltransferases are known to be generated in cells through cleavage at their stem regions (25), a mutant lGlcAT-P lacking the major part of its stem region (lGlcAT-PΔstem) was expressed to determine whether or not the mutant enzyme was cleaved. As expected, no cleavage product derived from lGlcAT-PΔstem was detected in the culture medium (Fig. 3*D*), indicating that GlcAT-P was cleaved at its stem region like other glycosyltransferases.

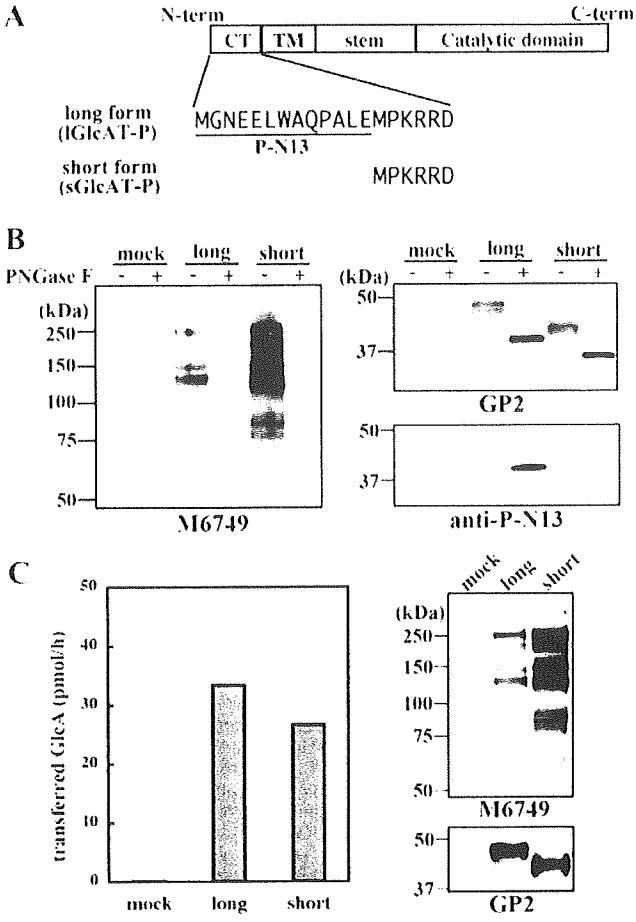


FIGURE 2. **Biosynthetic and *in vitro* glucuronylation activities of the two isoforms of rat GlcAT-P.** *A*, the two isoforms of GlcAT-P (lGlcAT-P and sGlcAT-P) differ in only the additional 13 amino acids (P-N13) in the N-terminal cytoplasmic tail. *B*, Neuro2A cells were transfected with the lGlcAT-P or sGlcAT-P expression plasmid or the empty vector (*mock*). Cells were lysed and treated with or without PNGase F and then subjected to Western blotting with M6749 mAb (*left*), GP2 (anti-GlcAT-P catalytic region) pAb (*top right*), or anti-P-N13 pAb (*lower right*). *C*, *in vitro* glucuronyltransferase activity toward a glycoprotein acceptor, asialo-orosomucoid, was measured. Mock treated-, lGlcAT-P-expressing, or sGlcAT-P-expressing Neuro2A cells were lysed and used as an enzyme source. The enzyme source solution was also subjected to Western blotting with M6749 mAb or GP2 pAb (*right*).

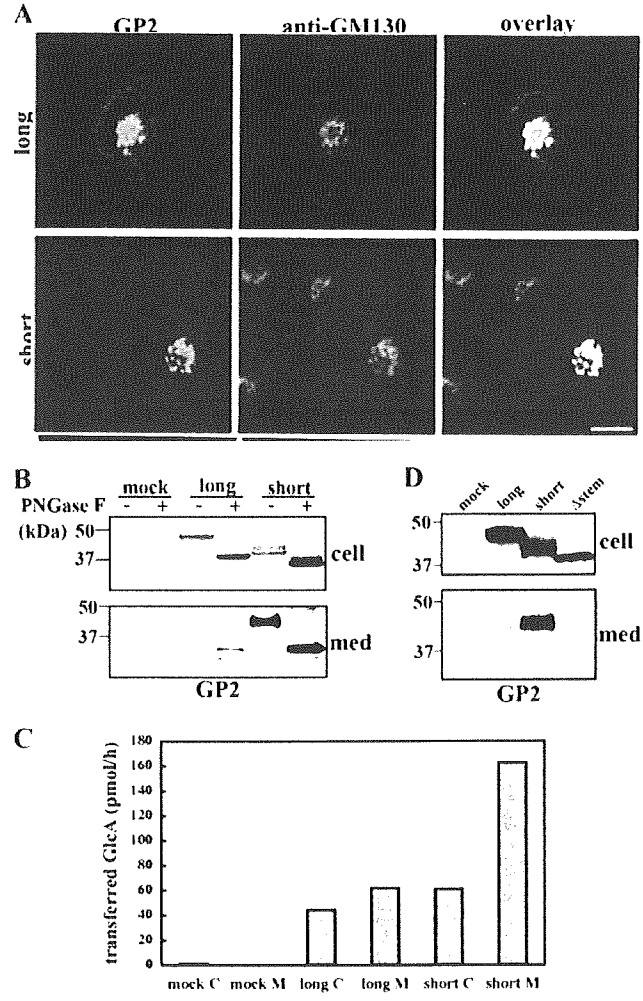


FIGURE 3. **Localization and secretion of the two isoforms of GlcAT-P.** *A*, Neuro2A cells expressing lGlcAT-P (*top*) or sGlcAT-P (*bottom*) were double-immunostained with GP2 pAb (*green*) and anti-GM130 mAb (*red*). The *right panels* show overlaid images. *Bar*, 10 $\mu$m. *B*, Neuro2A cells were transfected with the lGlcAT-P or sGlcAT-P expression plasmid or the empty vector (*mock*). Cellular proteins and proteins secreted into the culture medium (*med*) were treated with or without PNGase F and then subjected to Western blotting with GP2 pAb. *C*, *in vitro* glucuronyltransferase activity toward asialo-orosomucoid was measured. A mock-treated, lGlcAT-P-expressing, or sGlcAT-P-expressing Neuro2A cell lysate (*C*) or concentrated culture medium (*M*) was used as an enzyme source. Since the same volume of each enzyme source was used, specific activities in cell lysates and culture medium cannot be directly compared using the values. *D*, Neuro2A cells were transfected with the lGlcAT-P, sGlcAT-P, or lGlcAT-PΔstem expression plasmid or the empty vector (*mock*). Cell lysates and proteins secreted into the culture medium were Western blotted with GP2 pAb.

*Dibasic Motif Essential for Golgi Localization and Intracellular Activity of GlcAT-P*—As for the mechanism responsible for the distinct localization, secretion, and intracellular activity of the two isoforms of GlcAT-P, we investigated the role of a dibasic motif of glycosyltransferase in its transport. It was reported that some glycosyltransferases have a [K/R](*X*)[K/R] motif in their cytoplasmic tail proximal to the transmembrane border and that this motif was recognized by a small GTPase, Sar1, to transport glycosyltransferases from ER to the Golgi apparatus (16). They also showed that disruption of the motif caused the entrapment of glycosyltransferases, such as GalT2 or GalNAcT, in ER. GlcAT-P also has this motif in its cytoplasmic tail (Fig. 4*A*, KRR). If this motif of GlcAT-P is essential for its transport and localization, P-N13 of lGlcAT-P adjacent to this motif may affect GlcAT-P transport, leading to the distinct localization of the two isoforms. To determine the importance of this motif, a mutant lGlcAT-P lacking this motif (lGlcAT-P-AAA), in which the KRR sequence was substituted with AAA, was expressed (Fig. 4*A*). Immunostaining of the Neuro2A transfectant demonstrated that Golgi localization of lGlcAT-P-AAA was significantly disrupted, and the majority of the mutant was entrapped in ER (Fig. 4*B*), indicating a fundamental role of this motif in GlcAT-P. In addition, the disrupted localization of GlcAT-P led to a significantly low expression of the M6749 epitope compared with the wild-type enzyme (Fig. 4*C*, *left*), also confirming the necessity of the motif for GlcAT-P to serve as a functional glycosyltransferase. It was noticeable that lGlcAT-P-AAA was barely secreted (Fig. 4*C*, *right*), implying that the

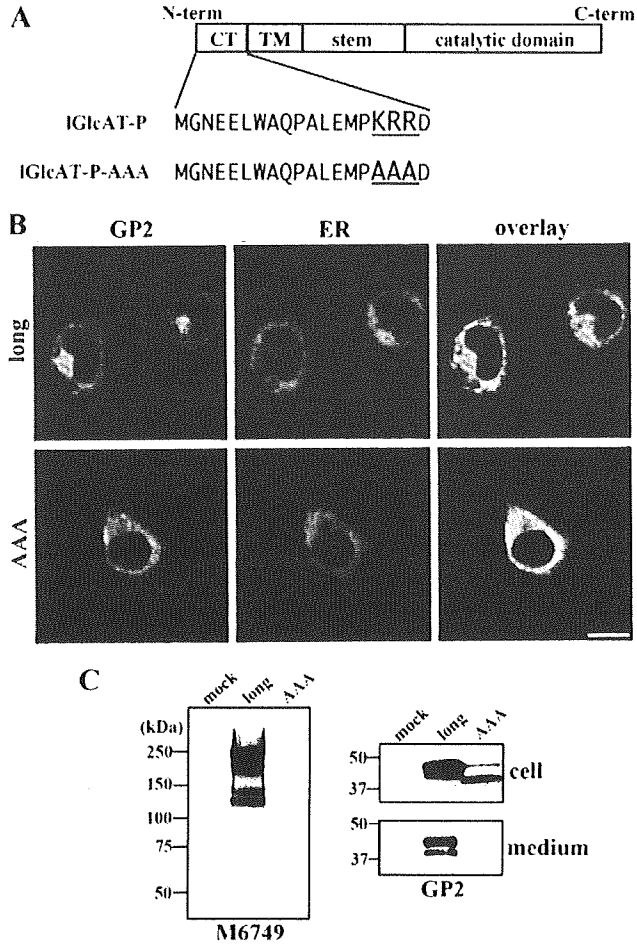


FIGURE 4. **Disruption of Golgi localization and intracellular activity of a mutant GlcAT-P lacking the dibasic motif.** *A*, in the cytoplasmic tail of GlcAT-P, a dibasic motif (KRR) exists. lGlcAT-P-AAA is a mutant lGlcAT-P lacking this motif. *B*, Neuro2A cells were co-transfected with the lGlcAT-P or lGlcAT-P-AAA expression plasmid and with pDsRed2-ER (Clontech). Cells were immunostained with GP2 pAb (*green*), and ER was visualized (*red*). Overlaid images are shown (*right*). *Bar*, 10 μm. *C*, Neuro2A cells were transfected with the lGlcAT-P or lGlcAT-P-AAA expression plasmid or the empty vector (*mock*). Cell lysates were Western blotted with M6749 mAb (*left*), and cell lysates and secreted proteins were Western blotted with GP2 pAb (*right*).

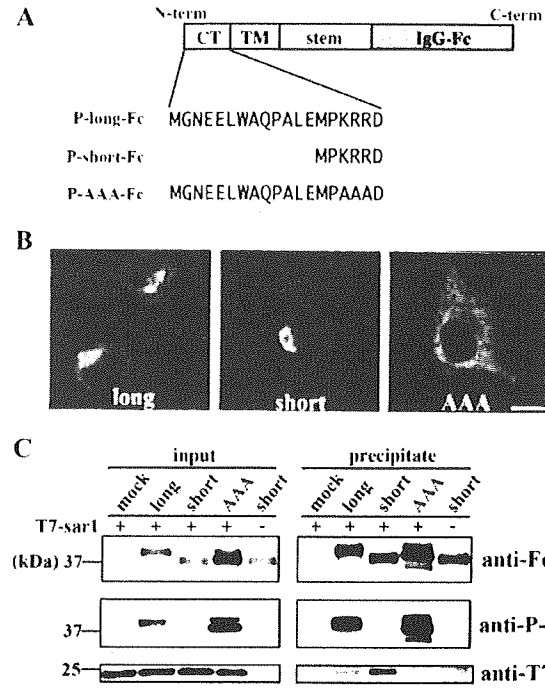


FIGURE 5. **Interaction between chimeric GlcAT-Ps and Sar1.** *A*, schematic diagrams of chimeric GlcAT-Ps are shown. The catalytic domains of these chimeras were replaced with the human IgG-Fc region. The N-terminal cytoplasmic tails of three chimeras, P-long-Fc, P-short-Fc, and P-AAA-Fc, correspond to those of full-length lGlcAT-P, sGlcAT-P, and lGlcAT-P-AAA, respectively. *B*, Neuro2A cells expressing P-long-Fc (*left*), P-short-Fc (*middle*), or P-AAA-Fc (*right*) were immunostained with anti-human IgG-Fc pAb. Note that the staining patterns shown here resemble those of the full-length enzymes (Figs. 2*A* and 3*B*). *Bar*, 10 μm. *C*, Neuro2A cells were transfected with the P-long-Fc, P-short-Fc, or P-AAA-Fc expression plasmid or the empty plasmid (mock). Cells were lysed and incubated with recombinant T7-tagged Sar1, followed by incubation with Protein G beads. The lysate mixture before precipitation (*left*) and the proteins precipitated with the beads (*right*) were Western blotted with anti-human IgG-Fc pAb (*top*), anti-P-N13 pAb (*middle*), or anti-T7 mAb (*bottom*).

cleavage of GlcAT-P occurred in the Golgi apparatus or in a subcellular compartment other than the ER.

*Distinct Interaction of GlcAT-P Isoforms with the Small GTPase Sar1*—Previously, the direct binding between Sar1 and the dibasic motif of a certain glycosyltransferase was shown (16). Therefore, we hypothesized that Sar1 also interacts with the KRR sequon in the GlcAT-P cytoplasmic tail, and P-N13 interferes with this interaction. To show this, we expressed a chimeric enzyme, GlcAT-P-Fc, whose catalytic domain was replaced with the human IgG-Fc region (Fig. 5*A*). As shown in Fig. 5*B*, these chimeric enzymes were localized in Neuro2A cells in almost the same way as the corresponding full-length GlcAT-Ps, indicating that from the N terminus to the stem region comprised a molecular determinant for the appropriate localization of this enzyme. Using these chimeric enzymes, the interaction with Sar1 was examined. Neuro2A cells expressing P-long-Fc, P-short-Fc, or P-AAA-Fc were lysed, and then T7-tagged Sar1 protein was added to the resultant lysate. After the precipitation of Fc-tagged enzymes with Protein G beads, the co-precipitated amount of T7-Sar1 was determined by Western blotting (Fig. 5*C*). Comparable amounts of the chimeric enzymes and an equivalent amount of T7-Sar1 existed in the mixture before precipitation, and anti-P-N13 blotting confirmed the expression of the chimeras with or without P-N13, as expected (Fig. 5*C*, *left*). In Fig. 5*C*, the *lower right panel* clearly shows that T7-Sar1 was co-precipitated with P-short-Fc much more than with P-long-Fc and that P-AAA-Fc, lacking the dibasic motif, was not co-precipitated with T7-Sar1. These results revealed that the dibasic motif in GlcAT-P was essential for Sar1 binding and that the existence of P-N13 weakened this interaction.

*Chimeric PST (ST8Sia-IV) Bearing P-N13*—To determine whether P-N13 had a similar effect on other glycosyltransferases, a chimeric enzyme, which was a polysialyltransferase, PST (ST8Sia-IV), fused with P-N13 at its N terminus, was expressed in Neuro2A cells (Fig. 6*A*). Polysialic acid (PSA), biosynthesized by PST (ST8Sia-IV) or STX (ST8Sia-II) (26, 27), is also a nervous system-specific carbohydrate, well known to be almost exclusively expressed on neural cell adhesion molecule,

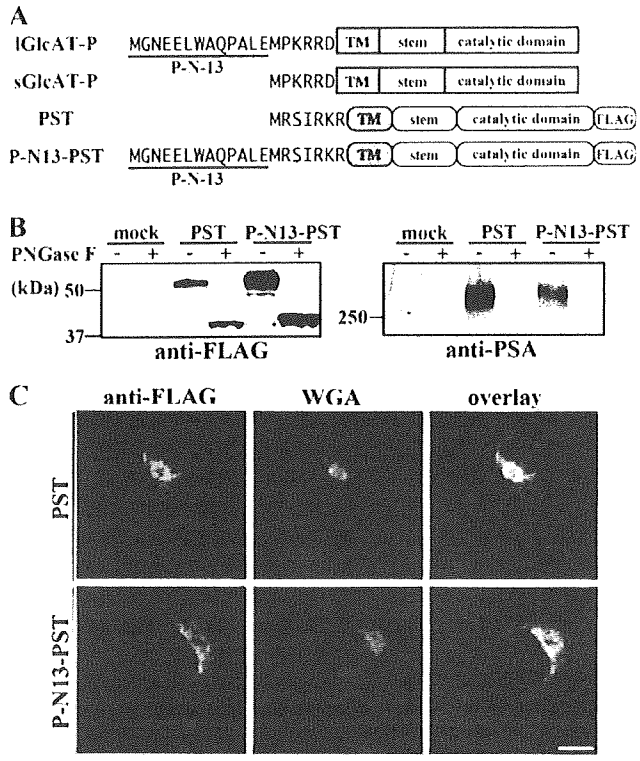


FIGURE 6. **Intracellular activity and localization of chimeric PST fused with P-N13.** *A*, schematic diagrams of 3×FLAG-tagged PST and chimeric PST are shown. The N-terminal cytoplasmic tails are depicted as the amino acid sequences. *B*, Neuro2A cells were transfected with the PST or P-N13-PST expression plasmid or the empty vector (*mock*). Cells were lysed and treated with or without PNGase F, followed by Western blotting with anti-FLAG mAb (*left*) or anti-PSA mAb (12E3) (*right*). *C*, Neuro2A cells expressing PST or P-N13-PST were co-stained with anti-FLAG mAb (*green*) and biotinylated wheat germ agglutinin lectin (*WGA*; Golgi marker; *red*). Overlaid images are shown (*right*). *Bar*, 10 $\mu$m.

and involved in synaptic plasticity (28). Since it was reported that Neuro2A cells expressed neural cell adhesion molecule endogenously (29), we are able to determine the level of PSA production by exogenously expressed PST in cells using Western blotting with anti-PSA antibodies. In addition, since PST has a dibasic motif in its cytoplasmic tail like GlcAT-P (Fig. 6*A*, RKR sequence), we can investigate the general roles of P-N13 in the regulation of glycosyltransferase localization and intracellular activity. C-terminal 3×FLAG-tagged PST or its chimera with P-N13 at the N terminus was expressed in Neuro2A cells, and then Western blotting with anti-FLAG or anti-PSA antibodies was performed (Fig. 6*B*). As shown in Fig. 6*B* (*right*), Neuro2A cells hardly expressed PSA endogenously, and the overexpression of PST produced PSA on *N*-glycans. The biosynthetic level of PSA was lower in P-N13-PST-expressing cells than in wild-type PST-expressing cells despite the higher enzyme expression (Fig. 6*B*). Moreover, co-staining with anti-FLAG mAb and Golgi marker wheat germ agglutinin lectin (30) showed that PST was mainly localized in Golgi, whereas P-N13-PST was not (Fig. 6*C*). These results were consistent with the intracellular activity and localization of sGlcAT-P and lGlcAT-P shown in Figs. 2 and 3, suggesting that the action of P-N13 was not GlcAT-P-specific but could also apply to other glycosyltransferases.

*Sequence-specific Role of P-N13*—As just described, the attachment of P-N13 to PST had effects on its localization and biosynthetic activity, as in the case of GlcAT-P (Fig. 6). However, it was a possibility that any peptide of 13 amino acids in length was capable of having a similar effect. To examine this possibility, another set of 13 naturally occurring N-terminal amino acids derived from the longer B4GalT-I isoform (G-N13) was attached to PST and sGlcAT-P (Fig. 7*A*). Unlike P-N13-PST, G-N13-PST exhibited Golgi localization (Fig. 7*B*) and biosynthetic activity comparable with that of wild-type PST (Fig. 7*C*). These results suggested that the effects of P-N13 were sequence-specific. Moreover, G-N13-GlcAT-P showed tight Golgi localization similar to sGlcAT-P (Fig. 7*D*), a relatively higher intracellular activity than lGlcAT-P (Fig. 7*E*, *left*), and higher production of the cleaved secreted form (Fig. 7*E*, *bottom right*), resembling the sGlcAT-P features. However, G-N13 also has a dibasic motif near the N terminus (Fig. 7*A*, RLR sequence, indicated by *dots*), and it is possible that G-N13 itself has an ability to transport glycosyltransferase to the Golgi apparatus. We expressed a mutant G-N13-GlcAT-P lacking the dibasic motif near the N terminus (G-N13AA-GlcAT-P) and revealed that G-N13AA-GlcAT-P exhibited significantly higher enzymatic activity in cells than lGlcAT-P (supplemental Fig. 1), indicating that the contribution of the dibasic motif in G-N13 was considerably lower than the inherent motif near the transmembrane border. Judging from these results for G-N13-PST and G-N13-GlcAT-P, P-N13 plays a specific role in the intracellular behavior of glycosyltransferase.

## DISCUSSION

In the present study, we demonstrated that the two isoforms of the HNK-1-sythesizing enzyme, GlcAT-P, differing in only the N-terminal cytoplasmic tail length, showed significantly distinct behavior, such as in localization, secretion, and HNK-1-producing activity in cells. Although the two isoforms were both functional in cells, as shown in Fig. 2*B*, their different intracellular activities could be a fine regulator of HNK-1 carbohydrate expression *in vivo*. These two isoforms were generated through alternative splicing in a conserved way in rodent and human brains (*i.e.* insertion right after the initiation codon generated an in-frame stop codon, resulting in the translation of the shorter enzyme, sGlcAT-P) (Fig. 1) (19, 20). Previously, we performed RT-PCR analysis using a brain RNA pool with primers in which the longer and shorter mRNAs were simultaneously and distinctly detected. As a result, although the precise ratios of the two mRNAs were not quantified, we revealed that lGlcAT-P is the major isoform in the mouse and rat, whereas sGlcAT-P is the major form in the human brain (19, 20). We do not know at present why the major isoforms are different among these species and whether or not the expression levels of the respective isoforms are regulated upon condition changes of cells, such as neural development and neurological disorder. However, if the proportion of the two isoforms of GlcAT-P changes under some cellular conditions, this probably results in a change in HNK-1 expression that can be explained by the different intracellular activities of the GlcAT-P isoforms.

Regarding the mechanism underlying the distinct localization of the two GlcAT-P isoforms, we focused on the ER exit